Glassy dynamics: From millihertz to terahertz

P. Lunkenheimer and A. Loidl

Abstract In this article, we review broadband dielectric spectroscopy in supercooled liquids, in many cases covering more than 15 decades in frequency and a wide range of temperatures from the low-viscosity liquid to the rigid sub-T_g glass. The access to this extremely broad frequency window allows a detailed study of the complexity of glassy freezing and glassy dynamics in a large variety of materials. Dielectric spectroscopy not only documents the enormous slowing down of the structural relaxation when approaching the glass transition, but also reveals a variety of further relaxation processes, which are important to understand the physics of the transition from a supercooled liquid into a rigid glass. After a short introduction, mainly focusing on long-term experiments on glasses and on the classification of glass formers into strong and fragile, we shortly discuss some basics of relaxation and conductivity contributions when viewed via dielectric spectroscopy. In chapter 3 we provide some prototypical examples of dielectric loss spectra covering a large frequency and temperature regime. The glass formers shown can be categorized into two classes, type A and type B. The latter reveal well-defined Johari-Goldstein secondary relaxations, which lead to peaks in the dielectric loss at least at low temperatures. The former exhibit an excess wing, showing only a change of slope of the high-frequency flank of the structural-relaxation loss peaks. Then we exemplify the phenomenology of glassy dynamics as revealed by these broadband spectra: the structural relaxation, the Johari-Goldstein relaxation, the appearance of a fast process as proposed by the mode-coupling theory, and the boson peak, a well-defined feature in the dielectric loss at THz frequencies, are discussed in detail. In a further chapter we focus on the importance of sub-T_g experiments: Aging experiments and a possible experimental evidence of the Gardner transition are discussed. Finally, we summarize the experimental dielectric results documenting the universality of glassy freezing, which can be directly derived from these measurements.

Keywords Dielectric spectroscopy, glassy freezing, Deborah number, structural relaxation, relaxation time, non-Arrhenius behavior, Johari-Goldstein relaxation, excess wing, fast process, boson peak, aging, Gardner transition

P. Lunkenheimer
Experimental Physics V, Center for Electronic Correlations and Magnetism
University of Augsburg, 86135 Augsburg, Germany
e-mail: peter.lunkenheimer@physik.uni-augsburg.de

A. Loidl
Experimental Physics V, Center for Electronic Correlations and Magnetism
University of Augsburg, 86135 Augsburg, Germany
e-mail: alois.loidl@physik.uni-augsburg.de

1. Introduction

Glasses are of outstanding importance in our daily life. The origins of glassmaking probably reach back to around 3000 BC where first glass beads were manufactured. Since then, glass formation plays a dominant role in many different areas: Not only for bottles, vessels, or windows in all types of architecture – from churches to skyscrapers – but also for polymers, biopolymers, metallic glasses, pharmaceuticals, optical cables, or fiber composites. Grain boundaries are a characteristic fingerprint of crystalline materials. The lack of grain boundaries in glasses, e.g., results in optical transparency in the case of silicate glasses or in superior mechanical stability in metallic glasses and is an outstanding property of the glassy state. Due to supercooling, glasses have a broad temperature window for processing. On the contrary, crystalline materials liquefy or solidify nearly instantaneously. It is a general believe that any substance can be supercooled into a glassy low-temperature state, either being small enough or being cooled fast enough. Sometimes liquids even do not crystallize at equilibrium. Binary mixtures of hard spheres with different radii are prototypical examples of the latter scenario [1].

It is a long-standing mystery that a glass is a solid without any long-range order and at the same time is a liquid that cannot flow. The question still has to be answered if the glassy state is a genuine state of matter [2]. When a liquid transforms into glass, its viscosity increases by almost 20 orders of magnitude and so does the average molecular relaxation time. However, the structure, when viewed via the pair correlation function, remains almost unchanged. How can an ensemble of atoms or molecules attain rigidity without breaking symmetry? When a liquid crystallizes in a first-order phase transition, symmetry is broken and ergodicity is broken: Disordered configurations are no longer available. If a liquid transforms into glass, ergodicity is broken, but the symmetry obviously remains the same and disordered configurations are frozen on almost infinite times. Of course, if supercooling can be viewed as a purely kinetic phenomenon, critical temperatures would be shifted to 0 K and whether a material behaves as a liquid or solid is a function of time, only. The Deborah number D, which measures the relation of relaxation time to observation time, is the only important quantity. If $D << 1$ the material behaves as a liquid, for $D >> 1$ as a solid [3]. Indeed, as expressed in the Old Testament in a song by the prophet Deborah (Judges 5:5), one might argue that, given enough time, all matter flows. In the Vulgate (the Latin version of the Bible) one can read: "*Montes fluxerunt a facie Domini*". Of course, this hypothesis can hardly be proven experimentally. Taking materials with relaxation times characterized by much shorter time scales can illustrate this behavior. Silly putty is an extreme example of such a material: It bounces like an elastic solid when dropped to a hard surface, but flows when put on a table for a couple of minutes under the action of gravity.

It has been speculated that old window glasses also will flow under the action of gravity and, hence, will be thicker at the lower edge when compared to the upper edge. This fact in some cases was verified in old medieval glasses, like, e.g., the window glasses of the cathedral in Augsburg from the end of the 11^{th} century, showing the prophets Hosea, Moses, Daniel, Jonas, and King David. However, even if so, it cannot be a proof of glass flow on long times. Zanotto [4,5] (see also the comment by Pasachoff [6]) calculated the flow of silica glasses and concluded that at elevated temperatures far above room temperature, the glass would move a visible amount in 800 years. However, at room temperature, any glass flow would appear on incredibly long times only, far exceeding human time scales. These calculations simply tell us that medieval artisans were clever enough to mount large window glasses with the thicker end at the bottom.

The pitch-drop experiment probably is the world's longest-term laboratory experiment to probe this liquid-solid duality of matter. This experiment was started in 1927 by Thomas Parnell at the University of Queensland to document that solid materials, in fact, on very long

time scales behave as liquids: At elevated temperatures, a sample of pitch was filled into a funnel, which then was sealed and was allowed to settle for three years. Then the neck was cut allowing the pitch to flow (Fig. 1) [7]. The first drop fell in December 1938 while the latest drop - number 9 - fell in April 2014. In the early days of the experiment, there was no special control of atmosphere or temperature, but in 1988, air conditioning was installed. The sequence of falling drops allowed to calculate the viscosity of the pitch at room temperature, which is approximately 2.3×10^{11} times that of water. Similar experiments have been also started in other places, e.g., the Dublin pitch-drop experiment [8] was set up in Trinity College in 1944.

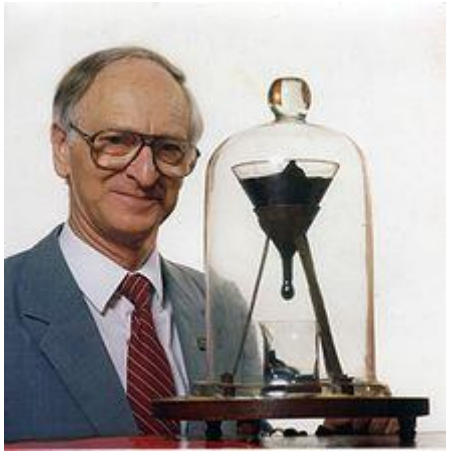

Fig. 1: The University of Queensland pitch drop experiment at 1990 two years after the seventh drop and 10 years before the eight drop fell. At that time, the experimenter was Professor John Mainstone. (Image Source: John Mainstone, University of Queensland).

That vitrification probably is much more complex and not at all a purely kinetic phenomenon only, comes from detailed experiments on viscosity of a large number of very different materials. When measuring viscosity or relaxation times as function of temperature over a large time or frequency range, one can observe two limiting behaviors [9,10,11]: Strong liquids follow an ideal Arrhenius behavior, $\eta \sim \exp(\Delta/T)$, where Δ corresponds to an energy barrier against molecular reorientation or displacement. At the lowest temperatures, viscosity grows towards infinity, but strictly only at T = 0 K. Window glasses based on amorphous SiO_2 are prominent examples approximately showing this so-called strong behavior. On the other hand, fragile liquids in an Arrhenius representation, log η vs. 1/T, are strongly curved, displaying so-called super-Arrhenius behavior. The viscosity in these cases can approximately be described by an Vogel-Fulcher-Tammann (VFT) law, $\eta \sim \exp[B/(T - T_{VF})]$, and diverges at the Vogel-Fulcher temperature T_{VF}, indicating some kind of low-temperature (hidden) phase transition at T_{VF}, well below the glass-transition temperature T_g, which is defined by a viscosity of 10^{12} Ps s or alternatively by an average relaxation time of ~ 100 s. Many low-molecular-weight glass formers, like ortho-terphenyl, follow this fragile temperature dependence of the viscosity.

This notably different relaxation characteristics is indicated in Fig. 2(a) in an Arrhenius-type representation, where the logarithm of the viscosity is plotted versus the inverse temperature [14]. The Arrhenius behavior yields infinite relaxation time at 0 K, while VFT behavior implies diverging relaxation rates at a finite temperature T_{VF}, which, however, is located well below the glass-transition temperature. The Arrhenius law implies a well-defined temperature-independent energy barrier against molecular motion, while a VFT behavior can be ascribed to temperature-dependent energy barriers E(T) [cf. dashed lines in Fig. (2b)]. The increase of the energy barriers on decreasing temperatures can be explained in terms of growing molecular clusters, which cooperatively reorient, and it seems clear that larger clusters will exhibit larger energy barriers as schematically indicated within the circles

at the right of Fig. (2b). This picture can be traced back to the early days of glass physics, where the super-Arrhenius behavior of the viscosity was explained by an increasingly cooperative character of molecular motions, in terms of growing cooperatively rearranging regions [12]. An experimental proof of growing length scales and, hence, an increasing number of correlated particles in approaching the glass transition, has been given recently by non-linear dielectric-susceptibility experiments [13,14].

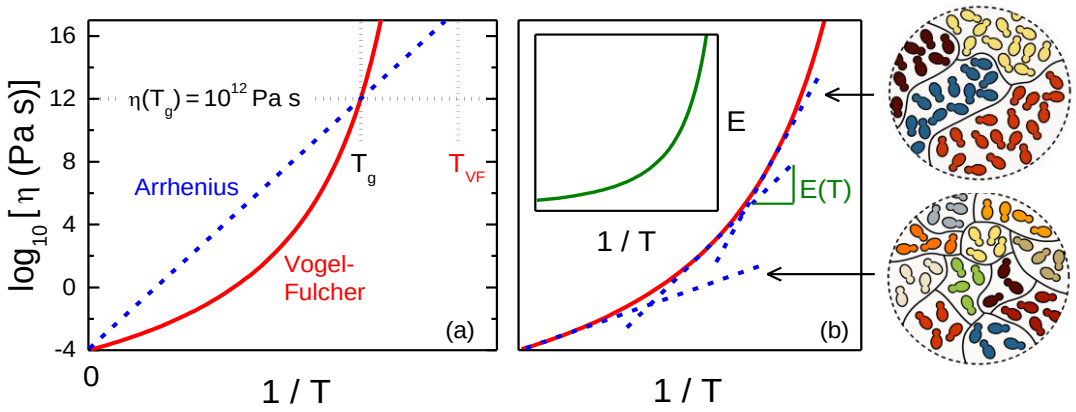

Fig. 2: (a) Temperature dependence of the logarithm of the viscosity of glass formers vs. the inverse temperature [14]. Strong liquids follow an Arrhenius behavior, while the temperature dependence of fragile liquids can approximately be described in terms of a Vogel-Fulcher-Tammann law. The two different behaviors are normalized at the glass-transition temperature T_g characterized by a viscosity of 10^{12} Pa s. The glass-transition temperature and the Vogel-Fulcher temperature T_{VF}, where the relaxation times become infinitely long, are indicated. (b) Vogel-Fulcher-Tammann behavior derived from temperature-dependent energy barriers E(T), which are explained in terms of growing molecular clusters, reorienting cooperatively, as schematically indicated by molecules of same color within the circles at the right [14]. The inset shows the temperature dependence of energy barriers vs. the inverse temperature, revealing the dramatic increase on decreasing temperature.

To summarize, the Arrhenius law of strong liquids implies a continuous increase in viscosity down to 0 K. In contrast, the VFT behavior signals a critical temperature. From early on, these two rather contradicting aspects, a purely kinetic freezing phenomenon vs. the assumption of a hidden phase transition, which, however, is not accessible in real experiments, guided the theoretical description of the glass transition over the last century. For example, some theories describe glasses simply as kinetically constrained liquids [15] with a strongly increasing viscosity, which makes them seem effectively rigid at low temperatures. Alternatively, other theories assume the existence on an underlying thermodynamic phase transition to a state with frozen-in but well-defined disordered positions [16].

2. Dielectric spectroscopy

To unravel the mystery of glass formation, the slowing down of molecular motion has to be recorded in the broadest dynamic regime possible. This can be achieved by dielectric spectroscopy, where 20 decades of frequency of the applied ac field can be covered. For this purpose, a vast number of different experimental techniques has to be employed, ranging from time-domain spectroscopy over frequency-response analysis and coaxial reflection/transmission methods far into the optical regime utilizing terahertz and far-infrared techniques [17,18]. Over the last decades, dielectric spectroscopy has been developed as an

extremely useful tool to unravel glassy dynamics [18,19,20,21,22,23]. These experiments do not only allow to categorize supercooled liquids into strong and fragile, but also demonstrated an enormous complexity of the relaxation dynamics, with the main structural relaxation accompanied by secondary relaxations, fast processes, and microscopic peaks in the optical regime. Dielectric spectroscopy has also been proven to be an ideal tool to study hole burning in supercooled liquids, an experimental proof of heterogeneity of the relaxation dynamics, excluding any homogeneous freezing scenario [24]. It is ideally suited to follow the ageing of glasses [25] and, in recent times, it even contributed to the dispute about the existence of a further transition, which is located deep in the glass state, the so-called Gardner transition [26]. Finally, non-linear dielectric spectroscopy has been developed and provided first hints concerning the cooperative character of glassy freezing [13,14,27,28]. These latter aspects will not be covered by this short review.

To characterize glassy matter, usually the complex dielectric permittivity $\varepsilon^* = \varepsilon' - i\varepsilon''$ is measured, which allows to determine the temperature and frequency evolution of the real part, ε', and the imaginary part, ε'', of the dielectric constant. When a material contains molecular dipoles and when its structure allows these dipoles to reorient, this molecular motion can be followed and mapped out by dielectric spectroscopy. Fig. 3(a) schematically shows the real and imaginary part of the dielectric constant as function of frequency for three different temperatures. On increasing frequencies, the dielectric constant exhibits a step-like decrease from a low-frequency "static" value, ε_s, to a high-frequency value, ε_∞, which is governed by the ionic and electronic polarizability of the material under investigation. A peak in the dielectric loss accompanies this step-like decrease of the real part. In the case of non-interacting relaxing dipoles, the loss peak is fully symmetric and has a width of 1.14 decades in frequency. This is the case of a pure Debye-like relaxation [29]. On increasing temperatures, the step in the real part and the peak in the imaginary part move towards higher frequencies, indicating the speeding up of dipolar reorientation, driven by thermal activation. The peak maximum (ν_p) and the point of inflection of the step-like decrease characterize the relaxation rate $\nu_\alpha = \nu_p$ or the relaxation time τ_α via the relation $\tau_\alpha = 1/(2\pi\nu_\alpha)$ and, hence, are a measure for the molecular mobility. The other important parameter of the Debye relaxation is the dipolar relaxation strength Δ, which is given by the height of the relaxation step or alternatively by the area under the loss peak.

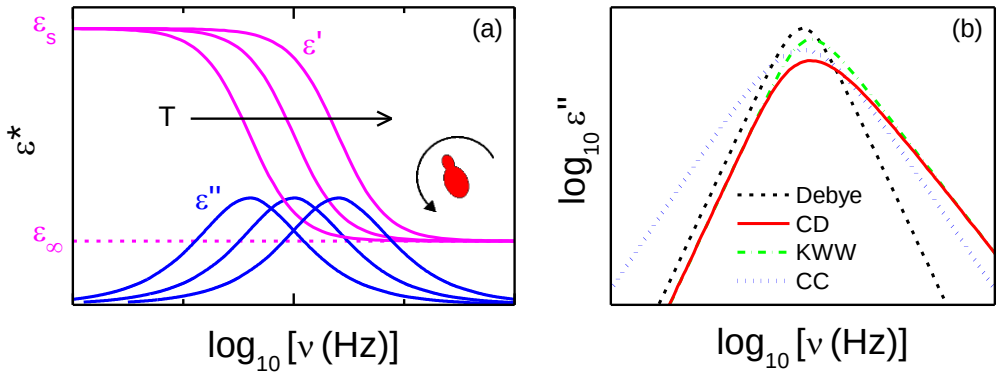

Fig. 3: Schematic view of the characteristics of dielectric spectra of glass formers as revealed by dielectric spectroscopy. (a) Typical relaxation spectra of real and imaginary part of the permittivity, shown for three temperatures. The horizontal arrow indicates increasing temperatures. The dashed line denotes the high-frequency dielectric constant. A molecular electric dipole, which via thermal activation can reorient, is indicated. (b) Model functions of the dielectric loss vs frequency on a double logarithmic plot. These functions are commonly used for the description of loss spectra: The symmetric Debye function, asymmetrically broadened Cole-Davidson (CD) and Kohlrausch-Williams-Watts (KWW) functions, as well as the symmetrically broadened Cole-Cole (CC) function are plotted (see text for details).

In the vast majority of real materials, dipolar relaxations, however, do not follow this Debye-like behavior. The loss peaks broaden considerably and in many cases have an asymmetric shape. Over the decades, several empirical functions have been developed to fit experimental data. The most common ones are the Cole-Cole (CC) [30], Cole-Davidson (CD) [31] and the Fourier transform of the Kohlrausch-Williams-Watts (KWW) function [32,33], to name a few. The dielectric loss calculated from these empirical functions is shown in Fig. 3(b) in addition to the Debye function. It is important to note that the asymmetrically broadened CD and KWW functions follow a pure Debye-like behavior on the low-frequency side of the peak, namely a linear increase of $\varepsilon''(\nu)$. The broadening can be explained assuming a distribution of relaxation times: Each molecule relaxes exponentially in a Debye-like fashion, however, with different relaxation times of molecules at different sites. Then, for the different functions mentioned above, an average relaxation time $\langle\tau_\alpha\rangle$ can be calculated. Usually, via $\langle\tau_\alpha\rangle \approx 1/(2\pi\nu_p)$ it can also be well approximated by deducing the peak frequency. The heterogeneous dynamics of the primary relaxation is treated in an enormous body of experimental and theoretical work, nicely summarized in Refs. [34,35,36]. However, also other scenarios are possible: For example, a temperature independent Gaussian distribution of energy barriers results in symmetrically broadened loss peaks, which can be described by the CC function. In this latter case, on decreasing temperature the width of these loss peaks would linearly increase following a 1/T behavior [26,37].

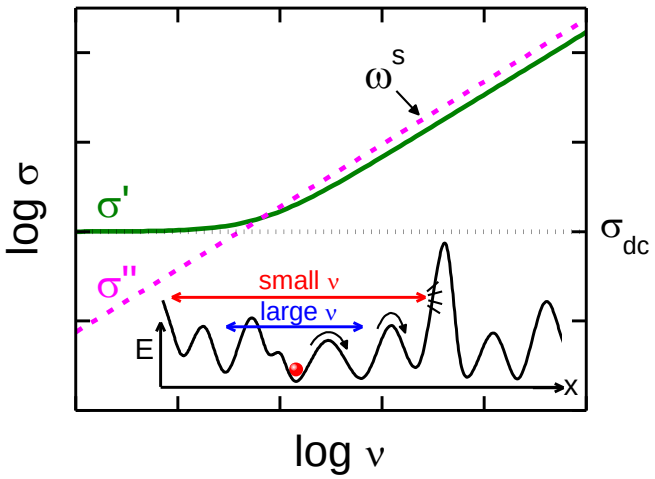

Fig. 4: Frequency dependence of real (σ', full line) and imaginary part (σ", dashed line) of the complex conductivity, plotted on a double-logarithmic scale. A dotted line indicates the frequency-independent dc conductivity. In the lower part of the figure, a schematic energy surface with a distribution of hindering barriers is indicated, illustrating the likely origin of the commonly observed increase of σ' with frequency.

In some cases, when a material contains mobile charge carriers like electrons or ions, the dielectric response is governed by charge transport. In these cases, it is better to describe the experimental results using a conductivity formalism. It should be noted, however, that there is a one-to-one correspondence between complex permittivity and complex conductivity, which reads $\sigma^* = i\omega\varepsilon^*$, and, thus, in principle both representations contain the same information. A representative plot of the complex conductivity is shown in Fig. 4: The real part of the conductivity, σ', reveals frequency independent dc contributions at low frequencies, crossing over into a pure ac conductivity towards higher frequencies. Ac conductivity contributions exhibit a characteristic power-law increase with frequency, $\sigma' \sim \omega^s$, with $s < 1$ [38,39]. The imaginary part of the conductivity is not sensitive to dc contributions and can be described by a similar power-law behavior with a different prefactor in the complete frequency range. The increase of the conductivity with increasing frequency results from the fact that the charge carriers, which are localized in potential minima with a broad distribution of energy barriers, at high frequencies easily can follow the applied ac electric field by back and forward jumps across small barriers. On the contrary, at low frequencies,

when moving over significantly larger distances, large barriers, which cannot easily be crossed, hinder them and long-range diffusion becomes suppressed (see schematic sketch shown as inset of Fig. 4) [40]. Here it should also be mentioned, that sometimes, especially for ionically conducting materials, instead of the conductivity representation the dielectric modulus $M^* = 1/\varepsilon^*$ is analyzed to characterize the ionic dynamics [41]. Spectra of the imaginary part $M''(\nu)$ reveal similar peaked behavior as $\varepsilon''(\nu)$ of non-conducting glass formers and can be analyzed in an analogous way. This enables the determination of the so-called conductivity relaxation time τ_σ, which is believed to provide a characteristic time scale for molecular motion in ionic conductors. However, one should be aware that the applicability and interpretation of the electric modulus is quite controversial (see, e.g., [42,43,44,45]).

Finally, we would like to come back to the temperature dependence of the average relaxation time of the primary relaxation, as observed in the vast majority of supercooled liquids. The structural or primary relaxation in glass-forming materials, as detected by dielectric spectroscopy, usually is called α-relaxation and, as will be shown later, is strongly coupled to the viscosity. In most glass-forming liquids, this strong coupling is valid for all temperatures above the glass-transition temperature and the dynamics of dipolar reorientation strictly maps the viscosity of the material under consideration. Of course, decoupling phenomena can appear below the glass-transition temperature, where molecular dipoles still may reorient, even in a rather rigid lattice. For the vast majority of supercooled liquids, with the prominent exception of mono-hydroxy alcohols [46], the α-relaxation is the dominating peak in frequency- and temperature-dependent dielectric spectra. Its tremendous slowing down under cooling in a narrow temperature range signals the increase in viscosity. As a rule of thumb, a viscosity of 10^{12} Pa s corresponds to a relaxation time of the order of 100 s.

As outlined already above and documented in Fig. 2, against naive expectations the viscosity and the average relaxation time, $\langle\tau_\alpha\rangle(T)$, in most supercooled liquids do not follow a simple Arrhenius law, $\langle\tau_\alpha\rangle = \tau_0 \exp[E/(k_BT)]$, which arises from purely thermally activated molecular motion over an energy barrier E separating neighboring minima in the potential surface of the system. Instead, for most glass formers a plot of $\log \langle\tau_\alpha\rangle$ versus 1/T exhibits significant curvature as indicated by the solid line in Figure 2(a), which sometimes is called super-Arrhenius behavior. It can be formally fitted by the empirical VFT formula, $\langle\tau_\alpha\rangle = \tau_0 \exp[DT_{VF}/(T-T_{VF})]$ [47,48,49]. Here D is the so-called strength parameter [50] and T_{VF} is the Vogel-Fulcher temperature. Small values of D imply strong deviations from Arrhenius behavior. Such glass formers are also termed “fragile”, in contrast to so-called “strong” glass formers, whose relaxation time more closely follows the Arrhenius law [50]. Alternatively, a fragility index m was defined, which is given by the slope of the relaxation times plotted versus T_g/T, just at the glass-transition temperature [51,52,53]. The strength parameter is related to the fragility index via $m \approx 16 + 590/D$. Hence, strong, Arrhenius-like behavior corresponds to a fragility index m = 16, while an upper limit of fragility was estimated to be close to 200 [54]. However, also other estimates exist (see later).

3. Glassy dynamics revealed by dielectric spectroscopy

In Figs. 5 and 6 we provide some prototypical dielectric broadband loss-spectra of materials exhibiting glassy freezing as measured during the last years in our group in different systems. All the spectra shown in these figures are a combination of the results of different techniques. As will be indicated, most of these spectra have been partly published, but in several cases are extended either in frequency or in temperature. They provide an impressive illustration of the slowing down of the structural relaxation in a variety of glass-forming systems, ranging from water-salt mixtures to various molecular systems, documenting the

universal aspects of glassy freezing. The spectra reveal the enormous slowing down of the average relaxation rate, documented by the maximum of the loss peak (α-relaxation), which reaches up to 14 decades in frequency in a relatively narrow temperature regime. It has been proven for a variety of supercooled liquids that the α-relaxation closely follows the temperature evolution of the viscosity (see later). Figs. 5 and 6 impressively document the power of dielectric spectroscopy, which allows to follow and detect glassy freezing over more than 20 decades in frequency.

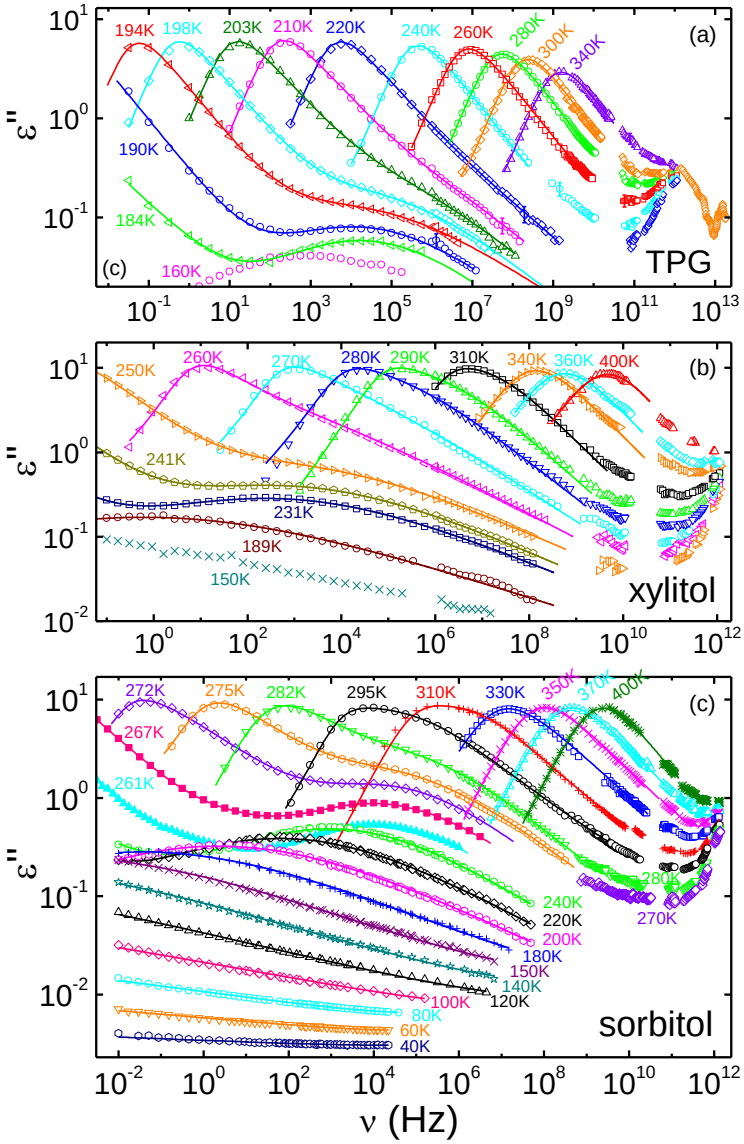

Fig. 5: Broadband dielectric loss spectra of so-called type B glass formers at a series of temperatures ranging from the low-viscosity regime down to the glass-transition temperature and below. All spectra are shown on double-logarithmic scales for a series of temperatures. The solid lines represent the sum of model functions for the α-relaxation and the JG secondary ß-process as described in the text. (a) tri-propylene glycol (TPG) [60,61], (b) xylitol [62], and (c) sorbitol [26,62]. In sorbitol, the dielectric loss is followed deep into the sub-T_g region.

In addition to the dominating α-relaxation, secondary processes appear at the high-frequency flank of the α-relaxation peak. There are numerous examples where secondary relaxations are peaked on the high-frequency flank of the structural relaxation and in these cases often are described as proto-typical examples of Johari-Goldstein (JG) relaxations [55]. The occurrence of these secondary processes is thought to be an intrinsic property of glass-forming liquids and to be inherent to the glassy state of matter. They do not, e.g., correspond to relaxations of side-groups of the molecules but may arise from relaxations in less-dense packed regions, so-called islands of mobility [55]. An alternative explanation ascribes JG relaxations to motions within a fine structure of the energy landscape experienced by the molecules [56,57,58].

Following the nomenclature introduced by the group of E. Rössler, these systems sometimes are termed type-B glass formers [59]. Three examples of broadband spectra of typical type-B glass formers are shown in Fig. 5.

The frequency and temperature dependence of tri-propylene glycol (TPG) is shown in Fig. 5(a). This spectrum covers more than fifteen decades in frequency. These results up to about 1 THz have been published by Köhler et al. [60]. Here we have added the high-frequency infrared spectra [61], which cover the boson peak and will be discussed later. This figure provides the main characteristics of the relaxation dynamics governing glassy freezing. At high temperatures, α-relaxation and boson peak are not well separated and almost merge. This fact shows that, at high temperatures in the low-viscosity limit, relaxational and vibronic time scales heavily overlap. On decreasing temperatures, the structural relaxation rapidly slows down, documenting the tremendous separation of time scales of relaxations and vibrations. A gap opens between the boson peak and the α-relaxation. However, the loss in between is strongly enhanced and cannot be described as a simple overlap of the low-frequency flank of the boson peak and the high-frequency flank of the structural relaxation [60]. In between a characteristic minimum appears, which represents a critical spectrum and is treated, e.g., in the framework of the mode-coupling theory (see later). At not too low temperatures (in the case of TPG for $T > 220$ K), the structural relaxation peaks up to the onset of the minimum can approximately be fitted by a CD function, yielding a constant slope of the high-frequency flank. However, at lower temperatures a clear peak evolves on this high-frequency flank, which becomes more prominent at low temperatures and is well established below $T_g \sim 194$ K. In Fig. 5(a) this sequence of α- and ß-relaxations are fitted by a sum of CD and CC functions, indicated by the solid lines in Fig. 5(a).

Similar spectra with a slightly reduced frequency scale are shown for xylitol [62] and sorbitol [26,62] in Figs. 5(b) and (c), respectively. The solid lines in Fig. 5(b) represent fits with a sum of Havriliak-Negami (HN) [63] and CC functions. The fits in sorbitol, indicated by solid lines in Fig. 5(c), were also performed utilizing a sum of HN and CC fits. Despite an overall similar behavior of the dielectric loss as function of frequency and temperature, there are significant differences when comparing these three dielectric loss spectra of type-B glass formers: The ß-relaxation in TPG has very low dipolar weight and on increasing temperatures seems to become almost hidden under the strong structural relaxation. The secondary processes in xylitol and sorbitol more strongly increase on increasing temperature and at elevated temperatures primary and secondary relaxations seem to be almost of equal weight. See, e.g., sorbitol at 295 and 310 K. The spectra of sorbitol are shown down to very low temperatures, far below T_g, and it is clear from these spectra that the ß-relaxation extremely broadens on decreasing temperatures. At the lowest temperatures, the dielectric loss is very low and characterized by a continuous decrease at least up to MHz frequencies. At 40 K the dielectric response is nearly flat, signaling an almost infinite width of the ß-relaxation, passing over into constant loss behavior [26]. These data can also be interpreted as signature of the so-called nearly constant loss, ascribed to a separate physical process. A prominent example is the "caged dynamics" treated within the extended coupling model [64].

Figure 6 provides three further examples of glassy freezing of supercooled liquids viewed via the dielectric loss, where secondary relaxations do not show up as well defined peak on the high-frequency side of the α-relaxation, but rather are indicated as change of slope, only. Fig. 6(a) shows the dielectric loss as measured in H_2O:LiCl solutions [65], Fig. 6(b) the results in glycerol [20] and Fig. 6(c) in salol [66]. These so-called type-A glass formers are characterized by a second, more shallow power law at the high-frequency flank of the α peak, termed "excess wing", a nomenclature introduced by our group [67,68]. Again, at high temperatures $T > T_c$ the structural relaxation seems to be characterized by one asymmetric loss peak, approximately described by KWW or CD functions. On decreasing temperatures, $T_g < T < T_c$, the excess wing evolves. This is, e.g., well documented in the

dielectric loss of glycerol and salol slightly above T_g: At 195 K and at 10^3 Hz in glycerol and at 228 K and 10^4 Hz in salol, the high-frequency flank of the α-relaxation reveals a clear change of slope. At further decreasing temperatures, e.g., at 179 K in glycerol and at 211 K in salol, well below the glass transition temperature, a clear shoulder-like curvature evolves, which seems to be the remainder of the JG ß-relaxation. Here it should be noted that these sub-T_g results had to be taken in thermodynamic equilibrium, which was reached after keeping the samples at the measurements temperature for up to five weeks [25,68,69]. As for several type-A glass formers in this way the excess wing was found to develop into a shoulder at low temperatures, it has been argued that this spectral feature is due to a JG relaxation, which is closer coupled to the structural relaxation than in type-B systems [68,]. This was later on corroborated by various other experiments [70,71,72,73].

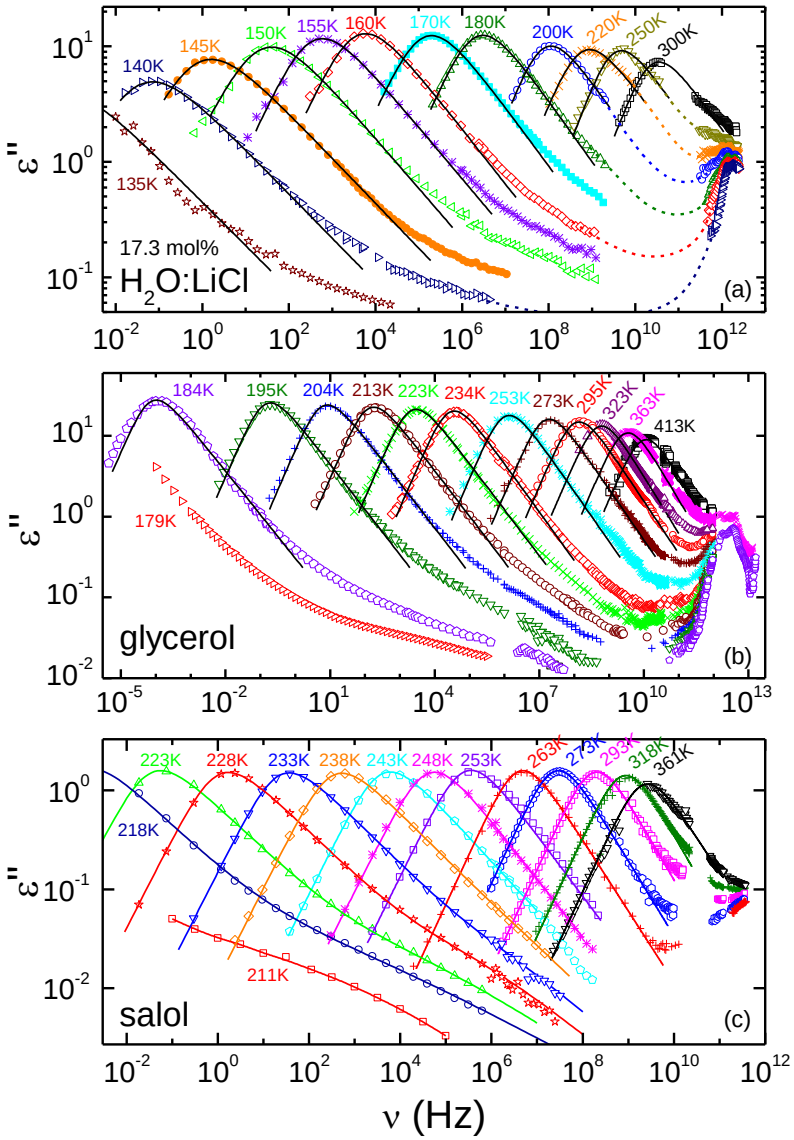

Fig.6: Broadband dielectric loss spectra of type-A glass formers. All spectra are shown on double-logarithmic scales for various temperatures. (a) 17.3 mol % water: LiCl solution [65]: the solid lines represent fits by a HN function for the α-relaxation. The dashed lines are drawn to guide the eye and to find a smooth extrapolation between the structural relaxation or the excess wing and the high-frequency peak. (b) glycerol [20]: the solid lines represent fits with a CD function for the α-relaxation. (c) salol [66]: the solid lines represent the sum of a HN function for the α-relaxation and a CC function for the secondary ß process. The line through the 211 K data is only a guide to the eye.

In what follows, we will describe in more detail the phenomenology of glassy relaxation as revealed in Figs. 5 and 6. In glassy matter, the tremendous increase in viscosity on decreasing temperatures is clearly mapped by the slowing down of the dielectric loss peak, shifting through the enormous frequency window in a relatively narrow temperature regime. Structural relaxation and microscopic processes in the THz regime overlap at high

temperatures. The microscopic processes remain almost temperature independent and on cooling a strongly temperature dependent minimum occurs at GHz frequencies, which is described, e.g., by mode coupling theory. At lower temperatures, JG secondary processes appear separating more and more from the structural relaxation approaching the glass transition temperature. This sequence of processes will be described in the following chapters.

3.1 Structural relaxation

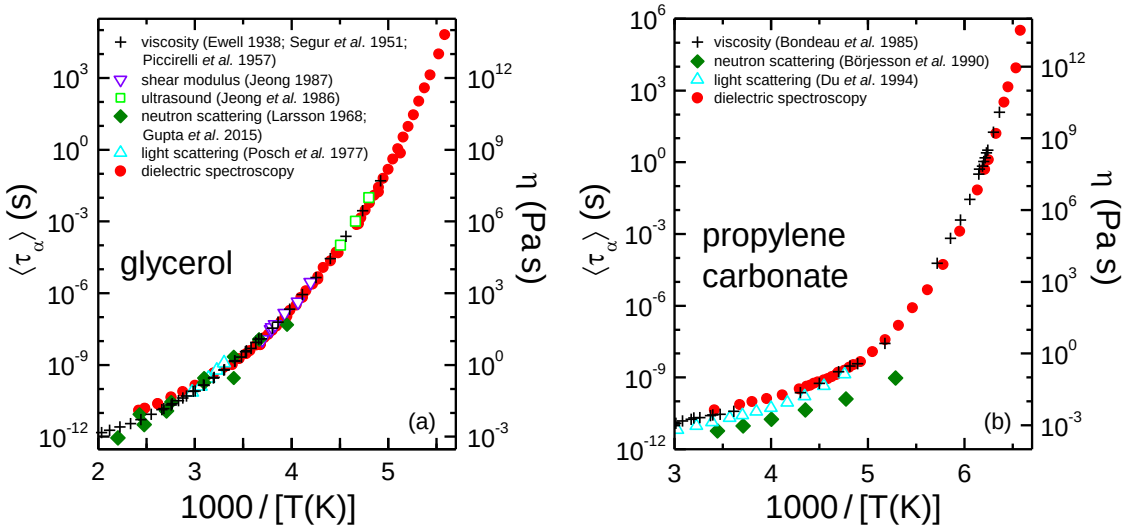

Fig. 7: Comparison of average relaxation times as determined by a variety of experimental techniques (left scale) compared with the temperature dependence of the viscosity (right scale) in (a) glycerol and (b) propylene carbonate [74]. The data for glycerol were taken from Refs. [75,76,77,78,79,80,81,82,83], those on propylene carbonate from [75,84,85,86]. The data are plotted in an Arrhenius-type representation. In both frames, the ranges of the axes of average relaxation times and viscosities were chosen to cover the same total number of decades and, in addition, their start values were adapted to match both data sets as close as possible.

As outlined above, the drastic increase of the viscosity of glass-forming materials is documented in the temperature evolution of the average relaxation rate ν_α or the corresponding relaxation time $\langle\tau_\alpha\rangle = 1/(2\pi\nu_\alpha)$. For temperatures above T_g, the temperature dependence of $\langle\tau_\alpha\rangle$ is strongly coupled to the viscosity and it can be measured by a variety of techniques, including ultrasound experiments, neutron and light scattering experiments, as well as by dielectric spectroscopy. For some systems, it has been experimentally checked if these average relaxation times really coincide with the temperature dependence of the viscosity, which of course is the true measure of glassy freezing. Examples are documented in Fig. 7(a) for glycerol and in Fig. 7(b) for propylene carbonate [74]. The most complete data set is available for glycerol. In Fig. 7(a) we compare our results of the average relaxation time as determined by dielectric spectroscopy in glycerol [75], with average relaxation times derived from shear modulus [76] and ultrasound results [77], as well as from neutron scattering [78,79] and light scattering experiments [80]. These average relaxation times are compared with existing viscosity results [81,82,83]. It is clear that viscosity results and relaxation times can be freely scaled against each other, however, only by a constant factor. In doing so, we find almost perfect agreement between all measurements in an astonishingly wide temperature and frequency regime. This figure also documents that the glassy dynamics can be studied by dielectric spectroscopy in the widest possible frequency range and with the

highest precision. If we take this comparison serious and accept the used scaling of viscosity and average relaxation times, we find that the glass transition temperature, which corresponds to a viscosity of 10^{13} Poise or 10^{12} Pa s determines an average relaxation time of 1000 s. As a rule of thumb, it is often assumed that the relaxation time at the glass-transition temperature equals 100 - 250 s.

Figure 7(b) provides a similar comparison for propylene carbonate. Here the average relaxation times as determined from our dielectric results [75], are compared with those deduced from neutron [84] and light-scattering studies [85]. Again, this temperature dependence of the average relaxation times is compared to the viscosity results [86] as described in detail in the figure caption. We find good agreement, with the exception that the neutron scattering data [84] seem to be significantly too low. If we accept scaling by a constant factor, we find that 10^{12} Pa s correspond to 10.000 s, which seems somewhat too large. Chen et al. [87] performed a critical comparison of viscosity and dielectric times. The main conclusion of their work was that rotational modes and viscosity are generally coupled, displaying parallel traces in the activation maps, although they can exhibit slight decoupling especially in the millisecond relaxation-time range. To conclude about the experimental facts documented in Figs. 7(a) and (b), we can state that the average relaxation times determined by dielectric spectroscopy certainly are strongly coupled to the viscosity and broadband dielectric spectroscopy is an ideal and unprecedented tool to study glassy dynamics.

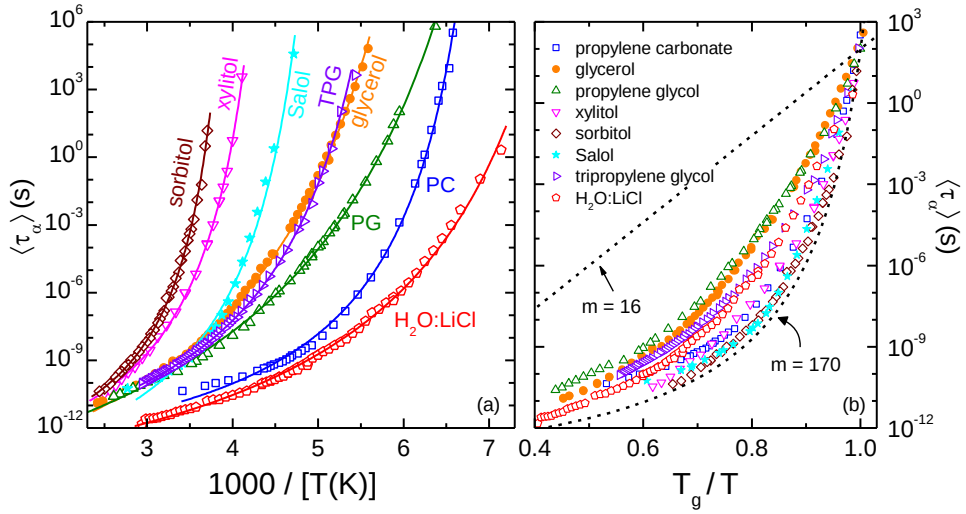

Fig. 8: a): Temperature dependence of average relaxation times in a variety of glass formers in an Arrhenius-type representation [65,75]: The logarithm of relaxation times is plotted vs. the inverse temperature. The solid lines represent fits with the Vogel-Fulcher-Tammann law (see text). b) Scaled relaxation times [21] in an Angell plot [89]: All materials shown are scaled to their glass-transition temperatures T_g. The dashed lines with m = 16 and m = 170 mark the extremes between strong (Arrhenius) and ultra-fragile behavior, respectively (see text).

The most relevant parameter that can be obtained from the loss peaks as documented in Figs. 5 and 6 is the average relaxation time. For the supercooled liquids shown in these figures, we collected the temperature dependence of the average relaxation times and added the results of propylene carbonate (PC) and propylene glycol (PC). The results are shown in Fig. 8(a). Lunkenheimer et al. [75] have collected most of these temperature dependencies of the average relaxation times. The $\langle\tau_\alpha\rangle$ values of the H_2O:LiCl solutions were taken from Ref. [65]. As indicated by the solid lines, the temperature evolution of the average relaxation times of this variety of different systems – in an extremely dynamic range – can rather nicely be parameterized by the VFT law. However, it has to be clearly stated that the VFT law is a mere parametrization of the temperature dependence of the average relaxation times, respectively

of the viscosity. There are a number of alternative approaches to model the temperature-dependent dynamics in glass-forming liquids. For example, Mauro et al. [88] have proposed an equation avoiding the divergence at a critical temperature inherent to the VFT law. In their formalism, the relaxations times, respectively the viscosity show a divergence at 0 K. Lunkenheimer et al. [75] provided a critical comparison of these two significantly different approaches, describing glass relaxation with or without the use of a critical temperature. They were able to show that in some cases this new Mauro-type temperature dependence really is superior. However, a number of examples were given, where the VFT law still provides the superior fits.

For a direct comparison, in Fig. 8(b) all average relaxation-time results presented in Fig. 8(a) are normalized to the glass transition temperature and are plotted on a scale T_g/T. In this so-called Angell plot [89], strong and fragile glass formers can easily be identified: The extreme values of strong and fragile are indicated by the dashed lines illustrating fragility indices of m =16 and m = 170. The value 16 corresponds to Arrhenius behavior, the value of 170 is indicated as the highest possible fragility index. This value has been adapted from Ref. [90] and is slightly lower than the fragility index m = 200 [53] cited above. The examples shown in Fig. 8(b) all rather belong to the fragile class of supercooled liquids, with sorbitol and salol being close to the fragile extreme.

3.2 Johari-Goldstein relaxation and excess wing

As noted above, characteristic secondary relaxations are observed on the high-frequency flank of the structural-relaxation loss peaks. In some cases, secondary relaxations stem from intramolecular modes, for example side-chain motions of polymers. From the viewpoint of glass physics, these relaxations are of minor interest. Here we are concerned with secondary relaxations, which are thought to be inherent to the glassy state of matter. In their seminal work [55], Johari and Goldstein documented that secondary relaxations are also found in glass-forming systems with rigid molecules, where side-chain motions are unlikely to exist. To discriminate these inherent secondary processes, which seem to be intimately linked to the structural relaxation, these processes are often termed Johari-Goldstein relaxations or, alternatively, slow ß-relaxations to distinguish them from the fast ß-process of the mode-coupling theory.

Figures 5 and 6 already document that these secondary relaxations, in the frequency domain, appear as distinct relaxation peaks (type-B glass formers) or just as a change of slope of the high-frequency wing of the structural relaxation, leading to the so-called excess wing [68] (type-A glass formers). However, it should be noted that it still is quite controversial if the excess wing is indeed due a JG relaxation, partly hidden in the spectra below the dominating α-relaxation [68,70,91], or if is due to an additional, separate relaxation process [59,92]. In type-B glass formers, these genuine JG relaxations appear as symmetric peaks. This is best documented in Fig. 5(c) for sorbitol. In type-A glass formers the maximum of the dielectric loss can hardly be observed and only the high-frequency wing of the JG-relaxation peak can be fitted. In most cases, these secondary processes are analyzed in terms of CC-type relaxations. In the temperature dependence of the dielectric loss, a significant contribution from the JG relaxation shows up, too. Figure 9(a) documents ε"(T) of sorbitol, a prominent example of a type-B glass former, for measurement frequencies between 10 mHz and 20 kHz [26]. The characteristic feature of the α-relaxation is a significant peak close to room temperature. On decreasing temperature, a second peak is observed, arising from the JG relaxation, well separated from the structural relaxation. It shifts to lower temperatures for lower measuring frequencies. It should be noted that in Fig. 9(a) a change of slope to a weaker temperature dependence of ε" is found below T_g. This feature is primarily due to the

sample falling out of thermodynamic equilibrium at the glass transition and less due to the onset of JG-relaxation contributions to ε"(T). In fact, especially for the two higher frequencies shown in Fig. 9(a) the JG relaxation also significantly contributes to the left flanks of the α-relaxation peaks at $T > T_g$, which can be easily verified by a comparison with the loss spectra in Fig. 5(c) at temperatures somewhat above T_g (e.g., 275 or 282 K).

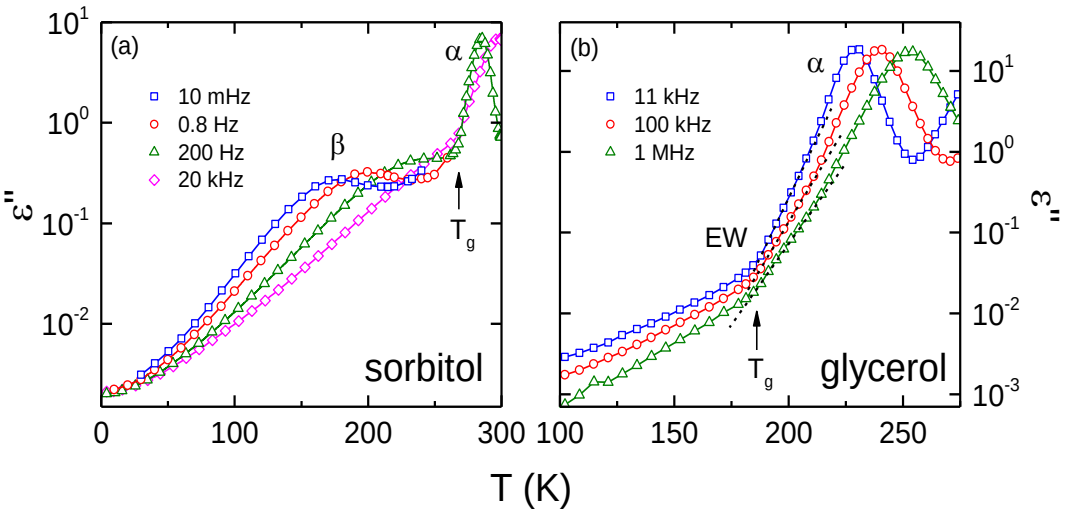

Fig. 9: Temperature dependence of the dielectric loss at selected frequencies in (a) sorbitol [26], a prototypical type-B glass former, and in (b) glycerol, a type-A glass-forming system. Both figures are shown on semilogarithmic scales. Arrows indicate the glass-transition temperatures in both materials. The dashed lines in (b) indicate excess wing (EW) contributions at temperatures > T_g.

In clear distinction to sorbitol, the secondary relaxation in glycerol [Fig. 9(b)] does not show up as a second peak in ε"(T). Glycerol belongs to the class of type-A glass formers and its loss spectra [Fig. 6(b)] show an excess wing on the high-frequency flank of the structural relaxation [68]. In the temperature dependence, the dielectric loss reveals two changes of slope. The first one, occurring at higher temperatures is induced by the onset of significant contributions of the excess wing to the loss, which exists already significantly above T_g. In Fig. 9(b) these contributions are indicated by the dashed lines. A second change of slope appears close to the glass transition temperature, where the systems falls out of thermodynamic equilibrium. Here the excess wing is completely dominating the dielectric response. As discussed above, there is no final consensus concerning the microscopic origin of JG relaxations. They could be interpreted as jumps between local minima in a multiwell energy landscape, e.g., local small-angle vibrations [56,57,58] or as local processes in less-dense regions of the structural glass, where, due to the frozen-in heterogeneity, islands of mobility exist [55].

From an evaluation of the frequency-dependent permittivity at different temperatures, it is possible to generate relaxation maps with α- and ß-relaxations in an Arrhenius-type representation. These are presented in Figs. 10(a) and (b) for two typical examples. Figure 10(a) shows the average relaxation times for sorbitol [62], which is a prominent type-B glass former. Below T_g, in these materials the secondary relaxations are well separated from the structural relaxation and strictly follow an Arrhenius-type of behavior. It is evident that this relaxation dynamics mostly appears in a frozen glass matrix, which is out of thermodynamic equilibrium. In sorbitol, the JG ß-relaxation decouples from the α-relaxation at temperatures well above the glass-transition temperature. It is not an easy task to analyze the temperature dependence of the ß-relaxation times for $T > T_g$, due to fact that the corresponding features in

the dielectric spectra strongly overlap and the resulting average relaxation times bear large experimental uncertainties. However, in literature there are some reports that τ of the ß-process passes through a shallow minimum before finally approaching the α-process [60,93,94]. Dyre and Olsen explained this minimum in terms of a so-called minimal model for ß-relaxations [93] while an "encroachment" of the relaxation time of an additional γ-relaxation with the JG relaxation was proposed in Ref. [95]. A minimum in the temperature dependence of the average relaxation time of the ß-process in sorbitol, before merging with the structural relaxation is compatible with the experimental results shown in Fig. 10(a) [62]. However, the precision of the data analysis does not allow finite conclusions.

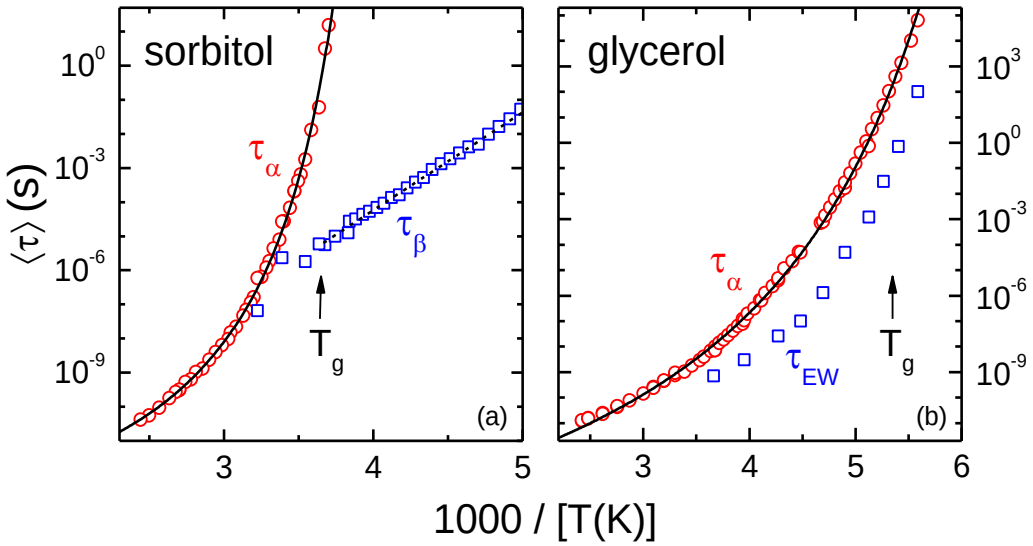

Fig. 10: Temperature dependence of average relaxation times of α- and ß-relaxation in an Arrhenius representation. Relaxation times are plotted vs. the inverse temperature for (a) sorbitol [62] and (b) glycerol [75,91]. The former is a type-B glass-former, the latter is of type A. The solid lines are fits with the VFT equation. The dashed line in (a) corresponds to Arrhenius behavior.

The temperature dependence of the secondary-relaxation times in type-A glass formers is significantly different: The secondary process, viewed via the excess wing, is always much stronger coupled to the structural relaxation. One problem arises because, in most cases, only the high-frequency flank of this secondary process can be analyzed and the tentative maximum is hidden under the dominating α-relaxation. An example where the secondary relaxation closely follows the primary relaxation in a distinct non-Arrhenius type of behavior is shown in Fig. 10(b) for glycerol [75,91]. This figure documents that the JG ß-relaxation in glycerol certainly follows a super-Arrhenius behavior and is closely coupled to the structural relaxation, in clear distinction to type-B glass formers. Fig. 10(b) also documents that the excess wing in glycerol can be analyzed well above the glass-transition temperature, even if large experimental uncertainties are considered. Similar results, namely that the JG relaxation is non-Arrhenius, were also found, e.g., for propylene carbonate, propylene glycol, and ethanol [60,91,96]. If the excess wing below the glass-transition temperature finally evolves into an Arrhenius behavior, cannot be finally decided. From the observations outlined above, one may conclude that the JG ß-process in type-B glass formers, at low temperatures strictly follows an Arrhenius behavior and at high temperatures probably exhibits a shallow minimum before merging with the structural relaxation. On the contrary, in type-A glass formers, the relaxation time of the excess-wing relaxation, also interpreted as inherent JG relaxation, always appears to closely follow the α-relaxation time, exhibiting an explicit super-Arrhenius

temperature dependence, and never seems to strongly decouple from the structural relaxation as found in type-B systems.

3.3 The fast process

The mode-coupling theory (MCT) [97,98,99] belongs to the most prominent theories of the glass transition. In 1984, Bengtzelius, Götze, and Sjölander [97] and, independently, Leutheusser [98] showed that a specific version of the MCT of liquids exhibits a dynamical singularity, with striking characteristics of the liquid-glass transition. This theory predicts, in addition to a critical slowing down of the structural relaxation, a fast process, sometimes termed fast-ß process, located in the GHz to THz frequency regime. This fast process is thought to be associated with a rattling motion of a particle dynamically caged by its neighbors in the supercooled liquid state. The rattling is responsible for the fast process at high frequencies while the decay of the transient cage corresponds to the structural relaxation at lower frequencies. Consequently, the generalized susceptibility exhibits a critical spectrum in the regime between the microscopic peak and the structural relaxation, which according to MCT follows specific scaling predictions, all of which are experimentally accessible and, hence, stimulated enormous experimental interest. A review on the variety of experimental tests of MCT predictions was given by Götze [100].

In frequency domain, in the transition region between the microscopic peak and the structural relaxation, the fast ß-process shows up as a significant minimum in the imaginary part of the susceptibility (which corresponds to the loss ε" in the dielectric case) with enhanced fluctuations. MCT predicts scaling laws for the temperature dependence of this minimum, namely for its frequency ν_{min} and the minimal susceptibility χ''_{min}. Moreover, the frequency of the peak maximum of the structural relaxation ν_α also should exhibit critical behavior with the critical exponents being determined by the shape parameters of the minimum (see below). First experimental records, proving that this critical spectrum with a significant self-similar enhancement above background noise really does exist, have been provided by neutron scattering [101] and light scattering [102]. In due course, the scaling behavior of this critical spectrum and the existence of a critical temperature T_c were verified by dynamic light [103,104,105,106] and quasielastic neutron scattering [105]. At that time, dielectric spectroscopy in the GHz to THz frequency regime in supercooled liquids was hardly accessible. Based on dielectric experiments in salol up to 10 GHz it was argued that there is no minimum in the dielectric spectra and, thus, that a critical slowing down and a critical temperature do not exist and that MCT predictions are invalid for dielectric spectroscopy [107]. However, due to the development of continuous-wave submillimeter and THz spectroscopy as well as advanced transmission and reflection techniques in the microwave range [18], it was later possible to measure the dielectric loss in this frequency regime of the critical spectrum with high precision and to prove the qualitative validity of MCT [108,109]. It should be noted that, in addition to MCT, there are also other approaches explaining the finding of a shallow susceptibility minimum at high frequencies. The most prominent example is the extended coupling model [64] where a nearly constant loss contribution is predicted, which is ascribed to "caged dynamics". Indeed, dielectric spectra including the region of the high-frequency minimum have successfully been fitted using this approach [108,110,111].

All the data sets determined from the different experimental techniques, like neutron and light scattering, as well as dielectric spectroscopy, finally yielded susceptibilities in qualitative agreement with MCT predictions, however also with sometimes quantitative differences. A critical comparison of the imaginary part of the dynamical susceptibility of glycerol, as measured by neutron and light scattering as well as by dielectric spectroscopy, is

provided in Ref. [19]. It covers the frequency regime of the critical spectrum including structural relaxation and microscopic peak. Similar comparisons have also be made for other glass formers [19,110]. Of course, it still is unclear to what extent MCT can be applied to real materials with irregularly shaped molecules and with very different microscopic intermolecular potentials. However, it is one of the main predictions of MCT that similar model parameters should arise from all observables, which couple to density fluctuations. In comparing the experimental results of neutron scattering, light scattering, and dielectric spectroscopy, one has to take into consideration that these experimental probes couple to different internal degrees of freedom: Dielectric spectroscopy and light scattering primarily probe the orientational dynamics of the molecules, while neutron scattering primarily couples to density fluctuations. One also should consider that MCT in its original form did not take into account non-spherical molecules and orientational degrees of freedom. Hence, perfect quantitative agreement between the results of these different experimental results cannot be expected. Later theoretical works, generalizing MCT by incorporating orientational degrees of freedom [112,113,114], have provided at least a qualitative understanding of many of these differences. Moreover, for supercooled propylene carbonate it was shown that the high-frequency susceptibilities from dielectric, light-, and neutron-scattering experiments can be consistently described within an extended mode-coupling approach [115,116].

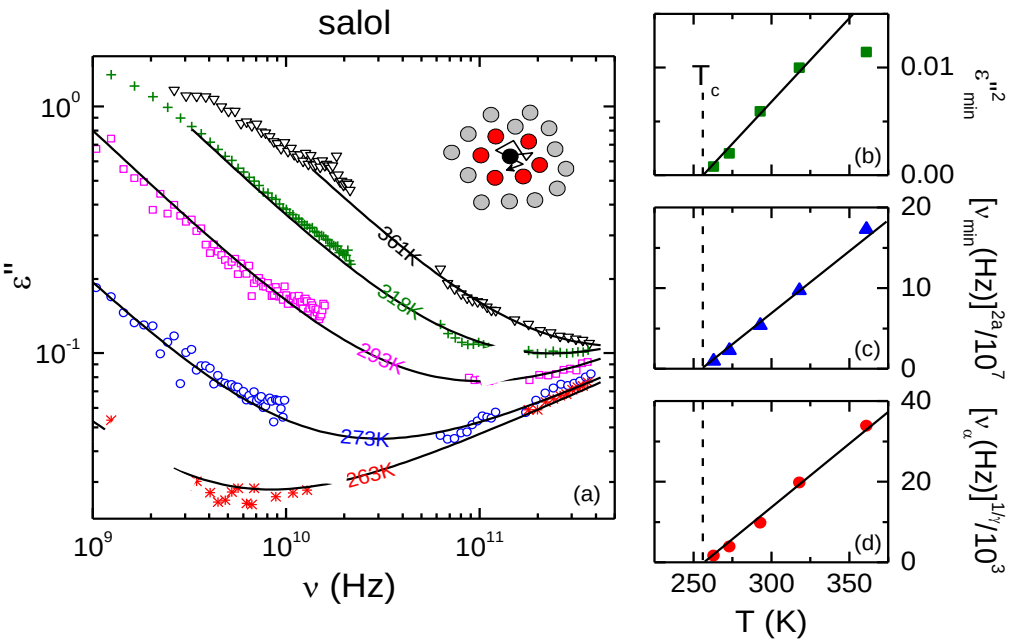

Fig. 11: (a) Dielectric loss of salol in the frequency regime of the fast ß process [61,117]. The solid lines are fits with the mode-coupling theory (see text). The inset shows a schematic sketch of the rattling process responsible for the frequency and temperature dependence in these regimes. Frames (b) - (d) show an analysis of these results within the framework of the mode-coupling theory: (b) temperature dependence of the minimum dielectric loss, (c) temperature dependence of the minimum frequency, and (d) temperature dependence of the structural relaxation rate [61,117]. Experimental results (symbols) are compared with theoretical predictions (solid lines). ε''_{min} is the minimum dielectric loss at a given temperature, ν_{min} corresponds to the frequency of the minimum, the exponent *a* corresponds to the high-frequency exponent of the minimum, ν_α is the relaxation rate of the structural relaxation and the exponent γ is given by $\gamma = 1/2a + 1/2b$, where *b* is the low-frequency exponent of the minimum.

Nowadays, the detection of glassy dynamics in this high-frequency regime by dielectric spectroscopy is well established and an example of the frequency and temperature dependence of the dielectric loss in the frequency regime of the critical spectrum is presented

in Fig. 11(a) for salol [61,117]. It shows the evolution of the dielectric loss ε" in the frequency regime between structural relaxation (< GHz) and microscopic peak (> THz) for temperatures between 263 and 361 K. Please note that the glass-transition temperature in salol is close to 220 K and, hence, all these measurements were performed well above T_g. It is well established that the dynamic liquid-to-glass phase transition as predicted by MCT appears at a critical temperature T_c, which is always located significantly above the glass-transition temperature. The dielectric loss of salol reveals the well-known susceptibility minimum. It can be well fitted by the MCT prediction, namely the sum of two power laws with an exponent $-b$, accounting for the increase towards the structural relaxation at low frequencies, and with an exponent a for the increase at high frequencies [solid lines in Fig. 11(a)]. We find exponent parameters a and b of 0.352 and 0.75, respectively. Both parameters are directly related to each other and temperature independent, i.e., the minima at different temperatures can be scaled onto each other. On increasing temperature, the minimum significantly shifts to higher frequencies and the minimum value of ε" strongly increases. According to mode-coupling theory, both quantities should follow strict scaling behaviors. An analysis of these results in terms of MCT scaling is documented in Figs. 11(b) – (d) [117]. The variation of the minimal dielectric loss ε''_{min} [Fig. 11(b)], the slowing down of the minimum frequency ν_{min} [Fig. 11(c)], and the predicted temperature dependence of the relaxation rate of the structural relaxation ν_α [Fig. 11(d)], all can nicely be described using the critical scaling predictions of MCT with critical exponents that are partly directly related to the exponents a and b deduced from the shape of the minimum. The critical behavior of all three quantities shown in Figs. 11(b) - (d) consistently points to the same critical temperature of T_c = 256 K. By light scattering, exponent parameters a = 0.327 and b = 0.641, as well as a critical temperature T_c = 256 K were determined [104], well consistent with the present results from dielectric spectroscopy. We these that these and similar results in other glass formers [19,21,60,108,109] really document the predictive power of mode-coupling theory and are a proof of the existence of a critical dynamic transition between the supercooled liquid and the structural glass. Lastly, we want to point out that the results of Fig. 11 finally settle the dispute on the presence of the high-frequency minimum and of the critical dynamics in the dielectric response of salol [104,107].

3.4 Boson peak

A rather intriguing, universal, and still highly controversially debated feature of disordered matter is the appearance of the so-called boson peak in vibrational spectra and thermodynamic properties. In heat-capacity experiments, it shows up as an excess contribution in the 10 K range. In vibrational spectra, this peak is revealed as an excess contribution to the density of states in the low THz range, which in crystalline materials usually exhibits a Debye-like ν^2 frequency dependence. The boson peak has been predicted to appear in Brillouin-scattering experiments in amorphous solids [118] and later on has been observed in a variety of disordered systems by Raman spectroscopy [119] and in inelastic neutron scattering experiments [120]. The name boson peak results from the fact that its amplitude exhibits only a weak temperature dependence, which obviously closely follows Bose-Einstein statistics. The boson peak can also be observed in dielectric spectroscopy and illuminating examples are shown in Fig. 5(a) for tri-propylene glycol and in Fig. 6(b) for glycerol.

Numerous models have been formulated to explain the microscopic origin of the boson peak and it is far out of the scope of this work to discuss and critically evaluate these vastly different models. Theoretical proposals include rather material-specific models [121], the involvement of soft anharmonic potentials [122], dynamics in fractal structures [123],

phonon scattering by intrinsic density fluctuations [124], spatially fluctuating force constants [125], random spatial variation of the shear modulus [126], or transverse vibrational modes arising from low-density defect structures [127]. It also has been proposed that the boson peak is a signature of a phase transition, where the potential energy surface changes from a minima-dominated phase with phonons to a saddle-point dominated phase without phonons [128].

As an example, in Fig. 12(a) we show the dielectric loss in glycerol in the frequency regime of the boson peak for a series of temperatures from 363 to 184 K, ranging from the low-viscosity liquid regime to the glass-transition temperature [129,130]. In glycerol, the boson peak is located at high frequencies, $\nu > 1$ THz, and is only weakly temperature dependent. At lower frequencies a strong temperature dependence appears, partly due to the superposition with the strongly temperature dependent structural relaxation, but partly also because in this frequency regime the region of the critical dynamics of MCT is entered [19]. Only at the lowest temperature shown in Fig. 12(a), at 184 K, the boson peak appears nearly unobscured, extending from about 0.5 to 10 THz. At frequencies above 10 THz, internal molecular vibrations are detected, which become narrow and well defined on decreasing temperatures. Astonishingly, the boson peak in glycerol seems to exhibit a double-peak structure, indicating that a complex density of vibrational states contributes to it.

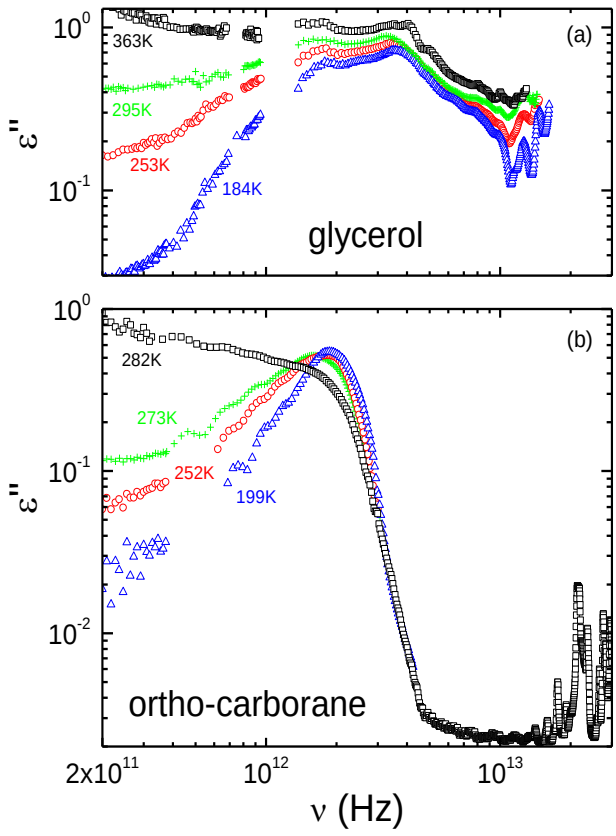

Fig. 12: Boson peak in (a) the supercooled liquid glycerol for temperatures between 184 and 363 K and (b) in the plastic crystal ortho-carborane at a series of temperatures between 199 and 282 K [130].

In Fig. 12 the boson peak in glycerol is contrasted with the corresponding feature as observed in a plastic crystal [130]. Plastic crystals are disordered systems, in which the centers of the molecules form a regular crystalline lattice and obey translational symmetry, while the orientational degrees of freedom are dynamically disordered and in some materials undergo glassy freezing into an orientationally disordered state [131]. Fig. 12(b) shows the boson peak in ortho-carborane for temperatures between 199 and 282 K [130]. Ortho-carborane is a highly symmetrical molecule and, at first sight, can be described as rigid

sphere. The rigid molecules form the analogue of a mono-atomic lattice and, hence, should be characterized by acoustic modes only. Intramolecular excitations appear above 20 THz and are well separated from the acoustic modes. In this case, it seems that the boson peak simply maps the acoustic density of states with a cut-off frequency close to 4 THz. In Ref. [130] it was speculated that the coupling to the THz radiation may arise from a disorder-induced breaking of selections rules or a strong hybridization of collective phonon modes with local relaxational excitations. In any case, Fig. 12(b) provides clear experimental hints that in the glassy, orientationally disordered state, the boson peak results from acoustic modes. On increasing temperatures, these modes become less and less well defined and finally merge with the relaxational mode close to 282 K.

4. Sub-T_g behavior of glasses

4.1 Physical aging

When a supercooled liquid is cooled below its glass temperature T_g, it falls out of thermodynamic equilibrium leading to the non-ergodic glass state. In the liquid state above T_g, under cooling the molecules (or other glass-forming entities like ions, atoms, polymer segments, etc.) can always adjust their arrangement in reaction to the falling temperature. However, this no longer is possible in the glass state because the relaxation time quickly reaches huge values below T_g (cf. Fig. 2) and, before the entities can adapt their arrangement, the temperature has fallen to even lower values. This results in a frozen glass state whose properties approximately reflect those of an equilibrium state at a higher temperature, termed fictive temperature T_f. Overall, this loss of equilibrium under cooling results in a weaker temperature dependence of various material properties below T_g as schematically indicated in Fig. 13. When, after cooling into the glass state, the material is held at constant temperature, in principle it will approach the equilibrium state. Then its properties will change with time, a process termed physical aging. This is indicated by the vertical arrow in Fig. 13. However, one should be aware that sufficiently far below T_g, due to the huge relaxation times arising already relatively shortly below T_g, this time dependence will be extremely slow and not detectable within realistic experimental time scales. Only for temperatures not more than several K below T_g, significant effects can be expected.

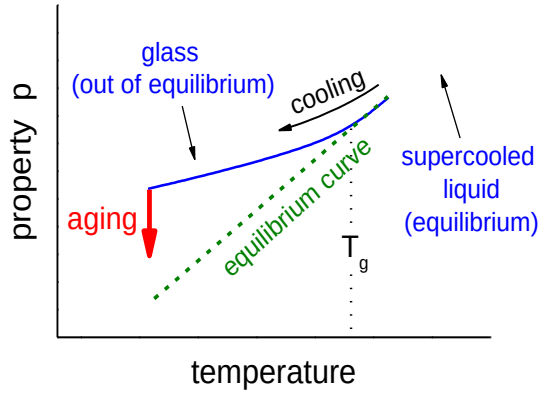

Fig. 13: Schematic plot of the temperature dependence of a material property around the glass temperature (solid line). When crossing T_g, a weaker temperature dependence is found. The dashed line shows the equilibrium curve. The vertical arrow indicates the approach of equilibrium under aging at constant temperature.

As an example, Figs. 14(a) and (b) show the time dependence of the dielectric loss of glycerol and xylitol under physical aging [25]. These experiments were performed after quickly cooling the samples from above T_g to temperatures about 6 K (glycerol) or 5 K (xylitol)

below the glass transition. Aging at constant temperature lasting up to 5 weeks was necessary to ensure that equilibrium was reached in these experiments. For both materials, a clear decrease of the dielectric loss is observed for all investigated frequencies. At these temperatures, the α peak is located outside of the investigated frequency range and ε"(t) in most cases reflects the behavior at the right flank of this peak. As discussed in Ref. [25], obviously the α relaxation shifts to lower frequencies under aging, resulting in the observed decrease of ε". For xylitol aging at 243 K, at the higher frequencies the β relaxation partly contributes to the detected loss [cf. Fig. 5(b)], which explains the partial crossing of the corresponding aging curves in Fig. 14(b) [25,132].

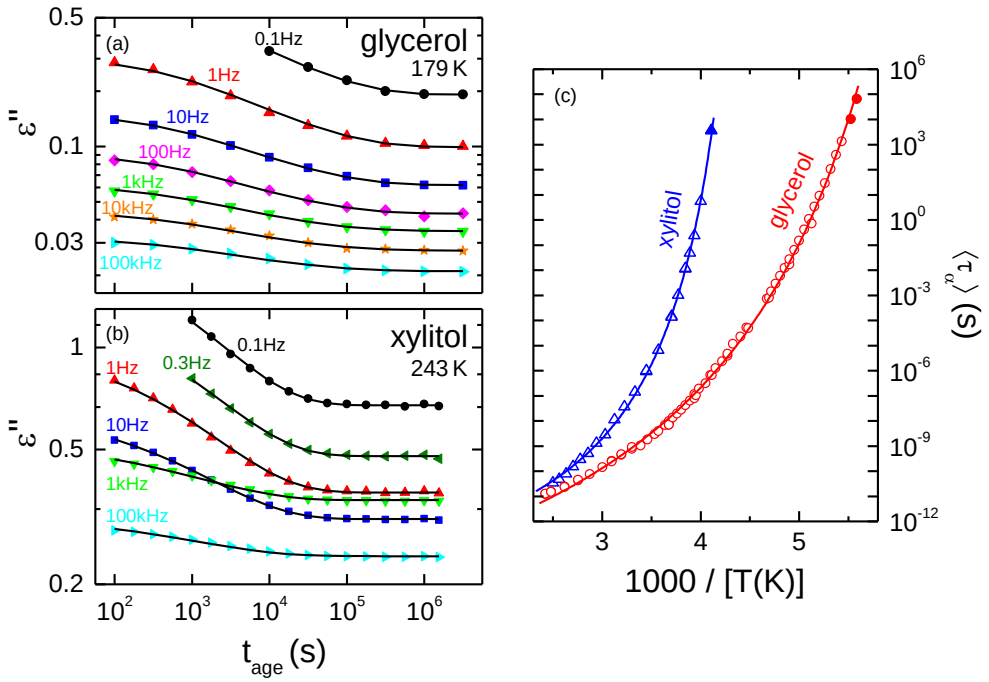

Fig. 14: Time dependence of the dielectric loss of glycerol (a) and xylitol (b) at temperatures below T_g [25]. The lines are fits with the modified KWW law as promoted in Ref. [25]. Frame (c) shows the average α-relaxation times determined from equilibrium experiments (open symbols) and the relaxation times deduced from the aging experiments, extending the equilibrium results by several decades (closed symbols) [25,75]. The lines are fits with the VFT function.

The analysis of such data is not straightforward. As realized already long ago, it is clear that, due to the structural rearrangements occurring during aging, the relaxation time of the material itself must be time dependent [133,134,135,136]. Therefore it is quite oversimplifying to fit such time-dependent data with simple stretched-exponential behavior with a fixed aging relaxation-time τ_{age} as done, e.g., in Refs. [137,138,139]. Clearly, the parameters obtained by such an analysis should not be compared with equilibrium results. For a more sophisticated treatment of such data, the Tool-Narayanaswamy-Moynihan formalism [133,134,140] can be employed, which traces back the aging-induced variation of properties to the time-dependent variation of the fictive temperature, leading to a time-dependent relaxation time. However, the application of this formalism is not straightforward and for rather simple aging experiments as in the present case, especially for aging triggered by a single temperature jump, our group has suggested an alternative phenomenological approach [25]. It assumes a stretched-exponential time dependence (also termed KWW behavior), however modified by introducing a time-dependent relaxation rate which itself also varies

with a KWW function. This ansatz can be solved by recursion and the lines in Figs. 14(a) and (b) are fits with this approach, excellently describing the experimental data. All $\varepsilon''(t)$ curves obtained at the different frequencies are simultaneously fitted with the same relaxation rate and width parameter, which is not possible when using a simple KWW function with time-independent τ_{age} [141]. Most importantly, only when employing this approach the obtained aging parameters are revealed to be consistent with those determined in equilibrium experiments at $T > T_g$ [25,132,142]. As an example, Fig. 14(c) shows the temperature-dependent α-relaxation times τ_α of glycerol and xylitol as determined from equilibrium measurements (open symbols) and, in addition, the relaxation times τ_{age} resulting from the analysis of the aging data (closed symbols) [25,75]. The latter provide a perfect extrapolation of the equilibrium data, thus extending the range of $\tau(T)$ by up to three decades. The stretching parameter of the KWW function deduced from aging also is consistent with the equilibrium results [25]. From these and similar findings in other glass formers [25,132], one can conclude that physical aging is governed by the same dynamics as the α relaxation and that $\tau_\alpha = \tau_{age}$.

4.2 Gardner transition

As outlined above, in the research field of the glassy state of matter there exists a long-standing controversy about a possible true phase transition and the existence of an ideal glass with infinite viscosity: The question if there is a hidden phase transition at non-zero temperature, which cannot be reached experimentally as the system falls out of thermodynamic equilibrium at the glass-transition temperature, or if glassy materials just become more and more sluggish on decreasing temperatures has finally not been answered. However, from an experimental point of view there is growing evidence of increasing length scales of cooperativity when approaching the glass transition [13,27,28], favoring a true phase-transition scenario. It came as a big surprise that recent theories suggest a further transition, deep in the glass state, which is thought to be even observable in non-equilibrium conditions. This so-called Gardner transition was originally predicted in mean-field theories of p-state spin glasses [143,144], but recently was also expected to exist in a variety of model glasses in infinite [145,146,147] as well as in three dimensions [148,149,150].The Gardner transition corresponds to a further fractionalization of the energy landscape making the glass even more heterogeneous in the low-temperature phase. However, it also has been argued that the Gardner transition might be strongly affected by finite dimensional fluctuations and doubts have been raised about its relevance for structural glass formers [151,152].

At the glass-transition temperature usually it is thought that the system is trapped in one of the many metabasins of the energy landscape and that the α-relaxation correspond to jumps between different metabasins. This scenario is indicated in Fig. 15(e) (left inset) at high temperatures. In real glasses, the structural relaxation slows down, its relaxation time following a VFT-type temperature dependence [solid line in Fig. 15(e)] and, approximately at the critical temperature T_c of mode-coupling theory, secondary JG relaxation processes decouple from the primary relaxation (dashed line). Within the metabasins these secondary relaxations can be thought as sub-basins, arising from local molecular motions [Fig. 15(e), middle inset]. At the hypothetical Gardner transition, a further roughening of the energy landscape occurs (right inset), which could give rise to a possible Gardner relaxation as indicated by the dash-dotted line in Fig. 15(e). Hence, in real glasses, the Gardner transition, if existent, has to be accompanied by a fractionalization of the JG sub-basins. As the Gardner transition can be also observed in non-thermodynamic equilibrium, it is clear that the experiment of choice is a detailed temperature dependent dielectric loss study of secondary

relaxations well below the canonical glass-transition temperature T_g. Long time ago this scenario has been proposed by Kirkpatrick and Wolynes [153]: Specifically with reference to the Gardner transition these authors pointed out that instabilities of the glass state at low temperatures may be associated with secondary relaxations.

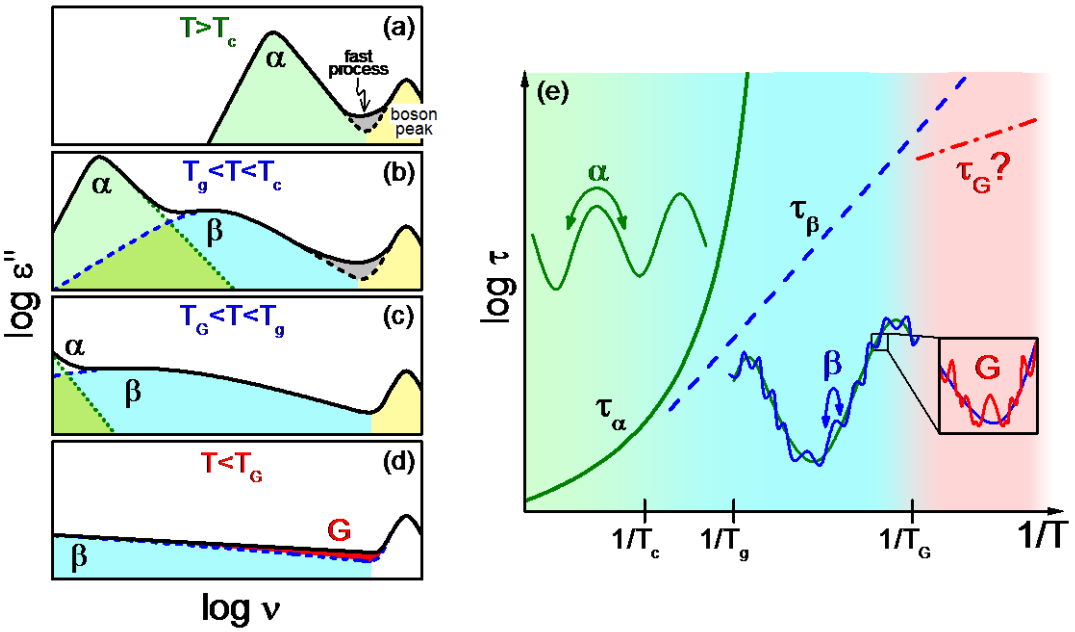

Fig. 15: (a-d) Schematic loss spectra vs. frequency of glass-forming materials on double logarithmic scales as function of temperature [26]: (a) The liquid state above T_c. (b) The supercooled liquid for $T_g < T < T_c$ with a well-developed secondary Johari-Goldstein relaxation. (c) The rigid glass below T_g but above the Gardner transition temperature T_G , $T_G < T < T_g$. (d) The glass far below the glass temperature and below the Gardner transition, $T < T_G < T_g$. The different dynamic processes are indicated by color: The α relaxation (green), the JG β-relaxation (blue), the fast process (grey), and the boson peak (yellow). The red area in (d) indicates the suggested additional contribution arising from the sub-basins in the energy landscape induced by the Gardner transition. (e) Typical temperature dependence of the α- and β-relaxation times in an Arrhenius plot with a possible additional Gardner relaxation arising below T_G [26]. In the different temperature regions we provide schematic views of the energy-landscape scenario: α-relaxation, JG β-relaxation, and possible modification of the local β-relaxation basins by the Gardner transition, leading to a fractal roughening of the landscape.

A scenario of the temperature evolution of the frequency-dependent dielectric loss including a possible Gardener transition is indicated in Figs. 15(a-d). (a): At temperatures above the mode-coupling T_c, in the highly viscous liquid phase, the mode-coupling critical dynamics appears between structural relaxation and boson peak. (b): Roughly at T_c, secondary relaxations decouple from the primary relaxation and shift through the frequency window in the supercooled liquid. (c): Below the glass-transition temperature T_g, the α-relaxation is shifted out of the experimentally accessible frequency window. Now all experiments are clearly out of thermodynamic equilibrium and only JG-type ß-relaxations can be observed. (d): On further cooling, the ß-relaxation considerably broadens and the mean relaxation rate of the secondary relaxation is also shifted out of the experimental frequency window, leaving only its high-frequency tail visible. Any further fractionalization of the energy landscape, the scenario of a possible Gardner transition, then can be assumed to yield additional loss contributions, as indicated in (d). In high-precision dielectric loss experiments it should be possible to identify this onset of excess loss at low temperatures and to relate it to the appearance of a possible Gardner transition.

In Fig. 5(c) we provided already broadband loss spectra of sorbitol in an extremely wide temperature range, including a detailed evolution of the secondary relaxation well below the glass-transition temperature [26,62]. Similar dielectric loss spectra are shown in Fig. 16 for xylitol [26]. In both glass formers, we find a strong shift of the β-relaxation peaks towards low frequencies accompanied by an extreme broadening. At the lowest temperatures, only the high-frequency flank of these secondary loss peaks can be detected. In Ref. [26], these loss peaks have been fitted using a Cole-Cole function, or, in case when the peak was completely shifted out of the frequency window of the experiment, by only fitting a power-law behavior accounting for the high-frequency flank. From these fits, it was possible to deduce the temperature evolution of the width parameter α of the symmetric CC function down to the lowest temperatures [26]. We want to point out that these experiments were performed at sufficiently low temperatures to exclude any effects from physical aging. As demonstrated, e.g., by Fig.14(b), detectable aging effects occur at temperatures much closer to T_g.

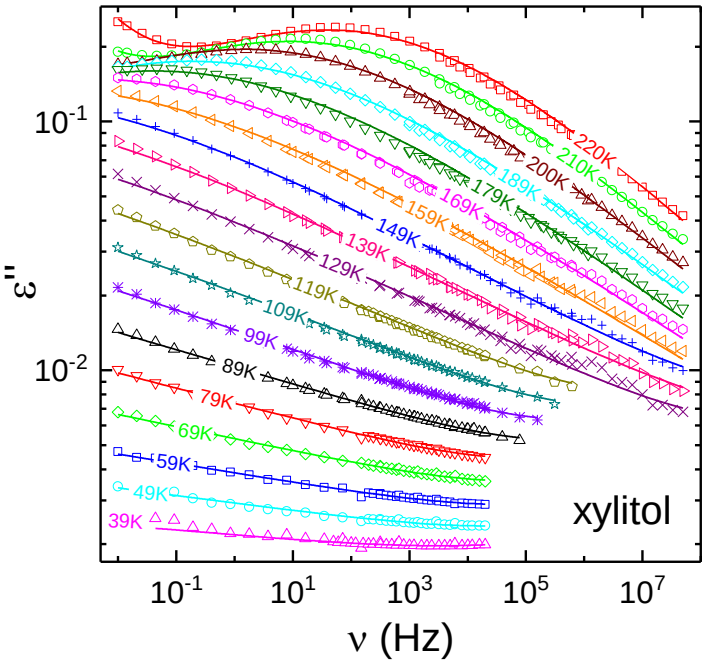

Fig. 16: Sub-T_g spectra of the dielectric loss vs. frequency of xylitol for various temperatures between 39 and 220 K [26]. The lines are fits by a combination of power laws and the CC function as described in the text and Ref. [26].

The analysis of the dielectric loss results of Fig. 16 reveals a strong increase of the width parameter on decreasing temperatures, nearly reaching unity at 0 K, as indicated in Fig. 17(a). One should have in mind that the approach of α = 1 on decreasing temperatures signals that the loss peaks become infinitely broad, resulting in a constant-loss behavior at the lowest temperatures. One possible scenario to explain this behavior relies on a model using a fixed distribution of local hindering barriers, namely assuming a temperature-independent Gaussian distribution of barrier heights [26,37]. This distribution characterizes the energy landscape of the sub-basins responsible for secondary relaxations as indicated in Fig. 15(e). That it is temperature independent follows from the fact that, below T_g, the local structure is effectively frozen-in. This model leads to symmetrically broadened loss peaks that closely follow CC behavior, justifying its application for the JG β relaxation. Interestingly, such a *temperature-independent* energy-barrier distribution leads to a strongly *temperature-dependent* distribution of relaxation times, namely, the half width W_τ of the latter is expected to diverge with 1/T [37,59]. From the experimentally determined width parameters of the CC distribution, shown in Fig. 17(a), the half widths W_τ were calculated and plotted in Fig. 17(b) [26]. Indeed, the overall behavior follows the general trend of a 1/T divergence. However, the line in Fig.

17(b), showing the expected $W_\tau \propto 1/T$ behavior, reveals some significant deviations. Here the proportionality parameter of the 1/T law was adapted to match the high-temperature data. Then $W_\tau(T)$, determined from $\alpha(T)$ of the loss peaks (circles), at low temperatures becomes even broader compared to the half width resulting from a constant Gaussian distribution of energy barriers (line). This strong additional low-temperature increase in the half width becomes even more obvious in the inset of Fig. 17(b) by plotting $W_\tau \times T$. As shown by the line in Fig. 17(a), the 1/T behavior of W_τ leads to an approximately linear increase of $\alpha(T)$. Again, deviations show up and the experimental width parameter approaches $\alpha = 1$ already at higher temperatures.

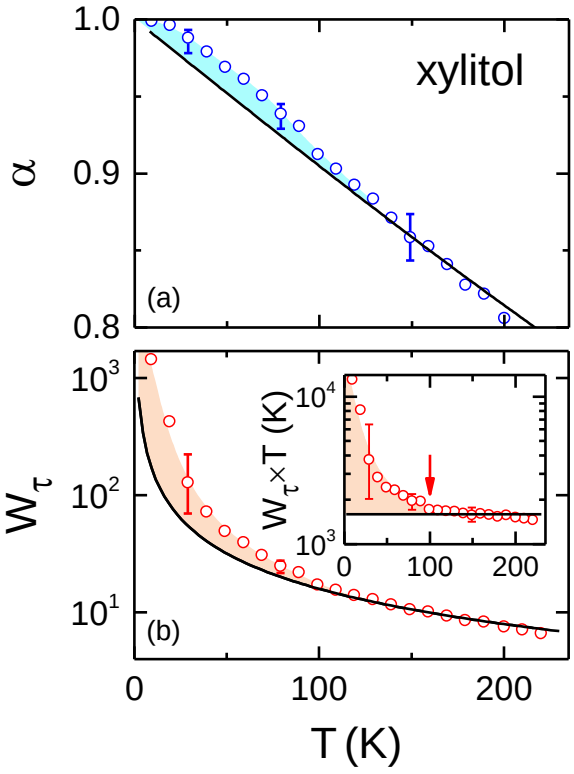

Fig. 17: (a) Circles indicate the temperature dependence of the width parameter α as obtained from fits of the dielectric loss of xylitol as described in the text [26]. The line was calculated from the 1/T dependence of W_τ shown by the line in frame (b). (b) The circles show the temperature-dependent half-width W_τ of the distribution of relaxation times, which was calculated from the experimentally determined $\alpha(T)$ assuming a temperature-independent Gaussian distribution of energy barriers. The line in (b) shows the expected 1/T divergence of W_τ, adapted to match the experimental data at high temperatures. The inset highlights the strong deviations from this expected behavior below approximately 100 K.

Geirhos et al. [26] interpreted this and similar behavior found for sorbitol as an indication of a further roughening of the energy landscape of the sub-basins by the Gardner transition. Based on these experiments, one can speculate that a Gardner transition indeed can be observed by a detailed study of secondary relaxations in real glass formers well below the glass-transition temperature and that in xylitol T_G is located approximately at 100 K. It is clear that these observed deviations of a continuously broadening JG relaxation may also have other reasons: In first respect one might argue that a constant Gaussian distribution of energy barriers is a too oversimplified approach and that the real distribution of energy barriers might be much more complex. In addition, constant-loss contributions due to caged dynamics have been predicted within the extended coupling model by Ngai [64]. It could well be that, at low temperatures, these additional constant-loss contributions superimpose with the loss of the high-frequency flank of the JG relaxations and finally become visible below 100 K in the case of xylitol. One has to await further experiments to further verify these speculations about the experimental observation of the Gardner transition in real glasses.

5. Concluding remarks on the phenomenology of glass freezing

In the previous chapters, we have discussed the phenomenology of glassy freezing as observed by broadband dielectric spectroscopy. For most supercooled liquids, the relaxation dynamics can be characterized by a dominating structural or α-relaxation followed in the spectra by an additional secondary JG-type process on the high-frequency flank of the α-relaxation peak. At GHz frequencies, we enter the frequency domain of the critical dynamics described by the mode-coupling theory, followed by the boson peak at THz frequencies. Intramolecular excitations at even higher frequencies have not been discussed in this review. A schematic overview of this complex relaxation dynamics is plotted in Figs. 18, depicting the situation for a rather low temperature, close to T_g [20]. Figure 18(a) shows the characteristic features of type-A glass formers, where the high frequency flank of the structural relaxation only exhibits a change of slope. We interpret this excess-wing phenomenon [68] as an inherent JG relaxation, which is more strongly coupled to the structural relaxation as compared to type-B glass formers and follows a super-Arrhenius behavior in its temperature evolution. Figure 18(b) shows the relaxation dynamics at a temperature close to the glass transition for a type-B glass former with the characteristic JG ß-relaxation. For temperatures $T < T_g$, the average relaxation time of the secondary relaxation strictly follows an Arrhenius behavior and is strongly decoupled from the structural relaxation.

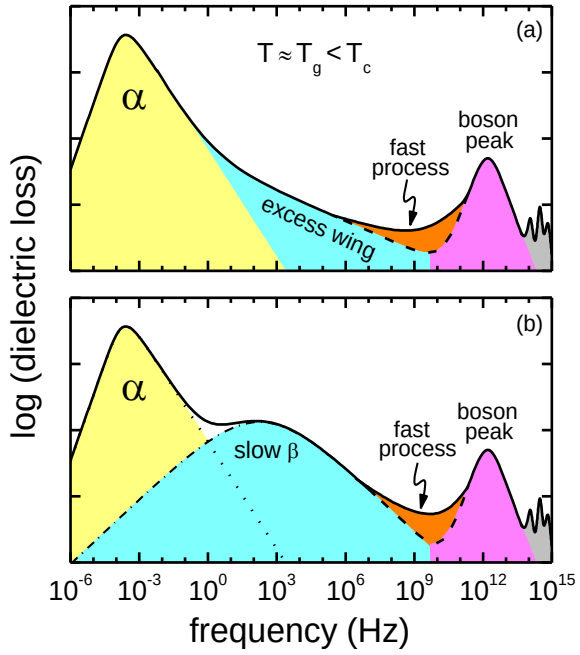

Fig. 18: Frequency dependence of the dielectric loss at a temperature close to the glass transition (a) in a prototypical type-A glass former with an excess wing and (b) in a type-B glass former with a canonical JG ß relaxation [20].

Finally, Fig. 19 provides the prototypical evolution of a supercooled liquid when cooled from a low-viscosity state at high temperatures to temperatures far below the glass transition [14,21]. At the highest temperatures [Fig. 19(a)], the dielectric loss of the low-viscosity liquid shows a dominant structural relaxation, almost merging with the boson peak. On lowering temperatures [Fig. 19(b)], and below the melting temperature T_m, the structural relaxation in the supercooled-liquid state separates from the fast processes creating a characteristic minimum, which is well described by the critical dynamics of the mode-coupling theory. This critical spectrum follows a strict scaling behavior with a critical temperature T_c. Of course, in real materials, this critical spectrum never softens completely and hopping processes play a dominant role. The dash-dotted line in Fig. 19(b) indicates a

possible CC peak responsible for the critical law [154]. Approximately for $T < T_c$, secondary relaxations evolve, which become more prominent on further lowering the temperatures. Figure 19(c) provides a schematic view of the relaxation dynamics close to the glass-transition temperature for a type-A glass former. The dash-dotted line indicates how the excess wing is caused by a submerged secondary relaxation peak [68]. Finally, well below the glass-transition temperature [Fig. 19(d)], only secondary relaxations survive. The dielectric loss in this temperature regime becomes almost flat and can be described as constant-loss phenomenon or as secondary process, which becomes infinitely broad. There are recent speculations that a further characteristic temperature appears below T_g, the Gardner transition [143], where the energy potential surface exhibits a further fractionalization [145,146,147,148,149], and that this transition gives rise to additional processes and can be identified by dielectric spectroscopy in sub-T_g experiments [26]. This has been detailed in chapter 4.2 and a schematic loss spectrum is shown in Fig. 15(d). Finally, the glassy freezing as viewed by dielectric spectroscopy via the dielectric loss [Fig. 19(a) – (d)] is confronted in Fig. 19(d) with the dielectric loss observed in a crystalline material. In a crystal with long-range translational and orientational order, phonons are the only relevant absorption processes and the idealized dielectric spectrum at low frequencies is completely loss-free.

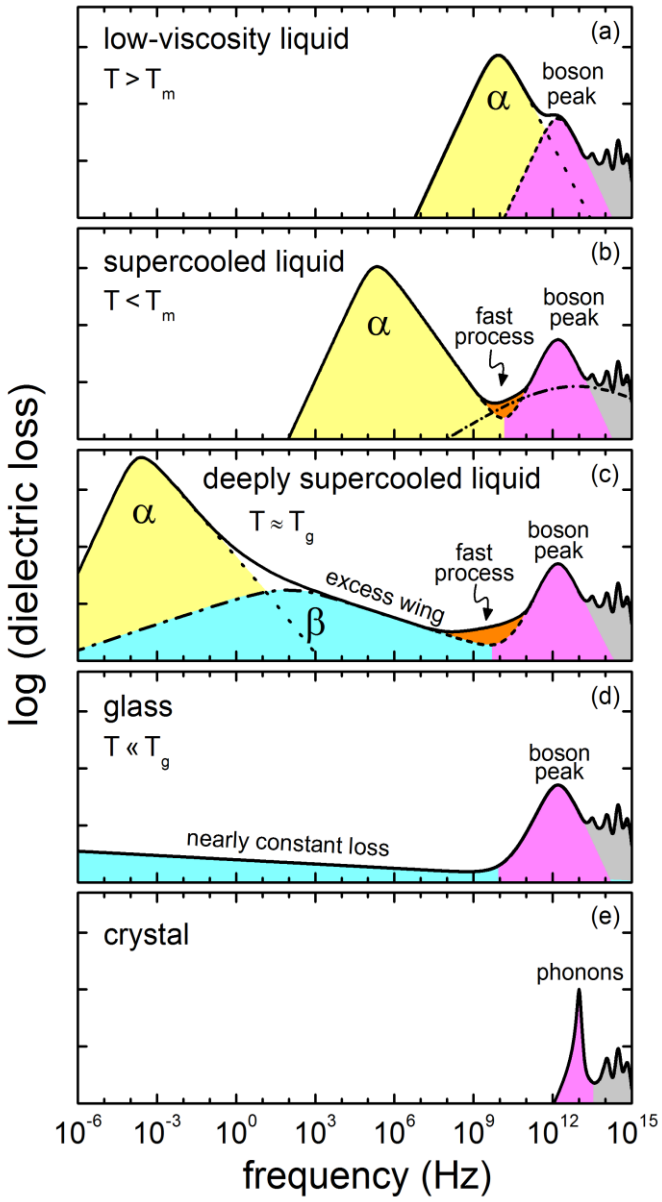

Fig. 19: Pictorial view of the temperature dependence of relaxation processes of supercooled liquids from the low-viscosity regime until deep into the glass phase, compared to the dielectric loss spectrum of an ideal crystal [14,21]. (a) In the low-viscosity liquid the structural relaxation almost merges with the boson peak. (b) In the regime of the supercooled liquid well above T_g, the structural relaxation and boson peak separate. In the minimum in between, the mode-coupling fast process emerges. The dash-dotted line indicates the CC peak discussed to be responsible for the critical dynamics [154]. (c) Close to the glass-transition temperature, a secondary β relaxation is observed. In the shown case of a type-A glass former, it leads to an excess wing. (d): At very low temperatures, in the sub-T_g regime, the structural relaxation is shifted out of the accessible frequency window. A nearly constant loss appears as a remainder of secondary relaxations. (e) Loss spectrum of crystalline matter, with long-range order. Here only phonons and intramolecular excitations exist.

In conclusion, we have documented in this short review the power of broadband dielectric spectroscopy to unravel the complexity of glassy freezing in supercooled liquids. The understanding of the temperature evolution of a variety of processes, including structural relaxation, Johari-Goldstein relaxation, the fast ß process of the mode-coupling theory, and the boson peak, which appear in very different frequency windows, are a prerequisite for a deeper understanding of the glass transition. One also should have in mind that, irrespective of the microscopic interpretations, glassy dynamics looks very similar in a variety of systems, spanning small-molecule glass formers, polymers, ionic melts, or plastic crystals. It seems that a universal freezing scenario governs the glass transition in all these very different materials. Finally, we have pointed out the significance of sub-T_g experiments, referring to the importance of aging and to recent experiments possibly indicating a further phase transition, the so-called Gardner transition, deep in the solid glass sate, which can be measured even in non-thermodynamic equilibrium.

[1] G. Parisi, Physica A **280**, 115 (2000).
[2] L. Berthier and M. Ediger, Physics Today **69**, 41 (2016).
[3] M. Reiner, Physics Today **17**, 62 (1964).
[4] E. D. Zanotto, Am. J. Phys. **66**, 392 (1998).
[5] E. D. Zanotto and P. K. Gupta, Am. J. Phys. **67**, 260 (1999).
[6] J. M. Pasachoff, Am. J. Phys. **66**, 1021 (1998).
[7] R. Edgeworth, B. J. Dalton, and T. Parnell, Eur. J. Phys. **198** (1984).
[8] R. Johnston, Nature News, 18.07.2014, DOI: 10.1038/nature.2013.13418.
[9] R. Böhmer, K. L. Ngai, C. A. Angell, and D. J. Plazek, J. Chem. Phys. **99**, 4201 (1993).
[10] C. A. Angell, K. L. Ngai, G. B. McKenna, P. F. McMillan, and S. W. Martin, J. Appl. Phys. **88**, 3113 (2000).
[11] R. Böhmer and C. A. Angell, in *Broadband Dielectric Spectroscopy* (F. Kremer and A. Schönhals, eds.), Springer, Berlin, 2003, p. 11.
[12] G. Adam and J. H. Gibbs, J. Chem. Phys. **43**, 139 (1965).
[13] S. Albert, Th. Bauer, M. Michl, G. Biroli, J.-P. Bouchaud, A. Loidl, P. Lunkenheimer, R. Tourbot, C. Wiertel-Gasquet, and F. Ladieu, Science **35**2, 1308 (2016).
[14] P. Lunkenheimer, M. Michl, Th. Bauer, and A. Loidl, Eur. Phys. J. Special Topics **226**, 3157 (2017).
[15] D. Chandler and J. P. Garrahan, Annu. Rev. Phys. Chem. **61**, 191 (2010).
[16] M. Dzero, J. Schmalian, and P. G. Wolynes, in *Structural Glasses and Supercooled Liquids: Theory, Experiment and Applications* (P. G. Wolynes and V. Lubchenko, Eds) J. Wiley, Hoboken (NJ), 2012, p. 193.
[17] R. Böhmer, M. Maglione, P. Lunkenheimer, and A. Loidl, J. Appl. Phys. **65**, 901 (1989).
[18] U. Schneider, P. Lunkenheimer, A. Pimenov, R. Brand, and A. Loidl, Ferroelectrics **249**, 89 (2001).
[19] P. Lunkenheimer, U. Schneider, R. Brand, and A. Loidl, Contemp. Phys. **41**, 15 (2000).
[20] P. Lunkenheimer and A. Loidl, Chem. Phys. **284**, 205 (2002).
[21] P. Lunkenheimer, M. Köhler, S. Kastner, and A. Loidl, in *Structural Glasses and Supercooled Liquids: Theory, Experiment and Applications* (P. G. Wolynes and V. Lubchenko, eds), J. Wiley, Hoboken (NJ), 2012, p. 115.
[22] R. Richert, Adv. Chem. Phys. **156**, 101 (2015).
[23] F. Kremer and A. Schönhals (eds), *Broadband Dielectric Spectroscopy*, Springer, Berlin, 2003
[24] B. Schiener, R. Böhmer, A. Loidl, and R. V. Chamberlin, Science **274**, 752 (1996).
[25] P. Lunkenheimer, R. Wehn, U. Schneider, and A. Loidl, Phys. Rev. Lett. **95**, 055702 (2005).
[26] K. Geirhos, P. Lunkenheimer, and A. Loidl, Phys. Rev. Lett, in press (arXiv: 1711.00816).
[27] C. Crauste-Thibierge, C. Brun, F. Ladieu, D. L'Hote, G. Biroli, and J.-P Bouchaud, Phys. Rev. Lett. **104**, 165703 (2010).
[28] Th. Bauer, P. Lunkenheimer, and A. Loidl, Phys. Rev. Lett. **111**, 225702 (2013).
[29] P. Debye, Ann. Phys. **39**, 789 (1912).
[30] K. S. Cole and R. H. Cole, J. Chem. Phys. **9**, 341 (1941).
[31] D. W. Davidson and R. H. Cole, J. Chem. Phys. **18**, 1417 (1950).
[32] R. Kohlrausch, Ann. Phys. **167**, 56 (1854).
[33] G. Williams and D. C. Watts, Trans. Faraday Soc. **66**, 80 (1970).

[34] H. Sillescu, J. Non-Cryst. Solids **243**, 81 (1999).
[35] M. D. Ediger, Annu. Rev. Phys. Chem. **51**, 99 (2000).
[36] R. Richert, J. Phys.: Condens. Matter **14**, R703 (2002).
[37] R. Böhmer, J. Chem. Phys. **91**, 3111 (1989).
[38] A. K. Jonscher, Nature (London) **267**, 673 (1977).
[39] P. Lunkenheimer and A. Loidl, Phys. Rev. Lett. **91**, 207601 (2003).
[40] J. C. Dyre, J. Appl. Phys. **64**, 2456 (1988).
[41] P. B. Macedo, C. T. Moynihan, and R. Bose, Phys. Chem. Glasses **13**, 171 (1972).
[42] S. R. Elliott, J. Non-Cryst. Solids **170**, 97 (1994).
[43] B. Roling, J. Non-Cryst. Solids **244**, 34 (1999).
[44] D. L. Sidebottom, B. Roling, and K. Funke, Phys. Rev. B **63**, 024301 (2001).
[45] I. M. Hodge, K. L. Ngai, and C. T. Moynihan, J. Non-Cryst. Solids **351**, 104 (2005).
[46] R. Böhmer, C. Gainaru, and R. Richert, Phys. Rep. **545**, 125 (2014).
[47] H. Vogel, Phys. Z. **22**, 645 (1921).
[48] G. S. Fulcher, J. Am. Ceram. Soc. **8**, 339 (1925).
[49] G. Tammann and W. Hesse, Z. Anorg. Allg. Chem. **156**, 245 (1926).
[50] C. A. Angell, in *Relaxations in Complex Systems*, edited by K. L. Ngai and G. B. Wright (Naval Research Laboratory, Washington, DC, 1985), p. 3.
[51] D. J. Plazek and K. L. Ngai, Macromolecules **24**, 1222 (1991).
[52] R. Böhmer and C. A. Angell, Phys. Rev. B **45**, 10091 (1992).
[53] R. Böhmer, J. Non-Cryst. Solids **172–174**, 628 (1994).
[54] T. A. Vilgis, Phys. Rev. B **47**, 2882 (1993).
[55] G. P. Johari and M. Goldstein, J. Chem. Phys. **53**, 2372 (1970).
[56] F. H. Stillinger, Science **267**, 1935 (1995).
[57] J. S. Harmon, M. D. Demetriou, W. L. Johnson, and K. Samwer, Phys. Rev. Lett. **99**, 135502 (2007).
[58] C. Gainaru, O. Lips, A. Troshagina, R. Kaghlau, A. Brodin, F. Fujara, and E. Rössler, J. Chem. Phys. **128**, 173505 (2008).
[59] A. Kudlik, S. Benkhof, T. Blochowicz, and E. Rössler, J. Mol. Structure **479**, 201 (1999).
[60] M. Köhler, P. Lunkenheimer, Y. Goncharov, R. Wehn, and A. Loidl, J. Non-Cryst. Solids **356**, 529 (2010).
[61] M. Köhler, *Relaxation, Rattling, and Decoupling. Dynamic Processes in Glassy Matter* (Mensch und Buch, Berlin, 2010).
[62] S. Kastner, M. Köhler, Y. Goncharov, P. Lunkenheimer, and A. Loidl, J. Non-Cryst. Solids **357**, 510 (2011).
[63] S. Havriliak and S. Negami, J. Polymer Sci. C **14**, 99 (1966).
[64] K. L. Ngai, J. Phys.: Condens. Matter **15,** S1107 (2003).
[65] P. Lunkenheimer, S. Emmert, R. Gulich, M. Köhler, M. Wolf, M. Schwab, and A. Loidl, Phys. Rev. E **96**, 062607 (2017).
[66] J. Bartoš, M. Iskrová, M. Köhler, R. Wehn, O. Šauša, P. Lunkenheimer, J. Krištiak, and A. Loidl, Eur. Phys. J. E **34**, 104 (2011).
[67] R. Brand, P. Lunkenheimer, U. Schneider, and A. Loidl, Phys. Rev. Lett. **82**, 1951 (1999).
[68] U. Schneider, R. Brand, P. Lunkenheimer, and A. Loidl, Phys. Rev. Lett. **84**, 5560 (2000).
[69] P. Lunkenheimer, R. Wehn, Th. Riegger, and A. Loidl, J. Non-Cryst. Solids. **307-310**, 336 (2002).
[70] A. Döß, M. Paluch, H. Sillescu, and G. Hinze, Phys. Rev. Lett. **88**, 095701 (2002).
[71] S. Hensel-Bielowka, S. Pawlus, C. M. Roland, J. Zioło, and M. Paluch, Phys. Rev. E **69**, 050501(R) (2004).
[72] J. Mattson, R. Bergman, P. Jacobsson, and L. Börjesson, Phys. Rev. Lett. **90**, 075702 (2003).
[73] T. Blochowicz and E. A. Rössler, Phys. Rev. Lett. **92**, 225701 (2004).
[74] U. Schneider, *Breitbandige dielektrische Studien der Dynamik struktureller Glasbildner* (Books on Demand, Norderstedt, 2000), ISBN 3-8311-0921-4.
[75] P. Lunkenheimer, S. Kastner, M. Köhler, and A. Loidl, Phys. Rev. E **81**, 051504 (2010).
[76] Y. H. Jeong, Phys. Rev. A **36**, 766 (1987).
[77] Y. H. Jeong, S. R. Nagel, and S. Bhattacharya, Phys. Rev. A **34**, 602 (1986).
[78] K. E. Larsson, Phys. Rev. **167**, 171 (1968).
[79] S. Gupta, N. Arend, P. Lunkenheimer, A. Loidl, L. Stingaciu, N. Jalarvo, E. Mamontov, and M. Ohl, Eur. Phys. J. E **38**, 1 (2015).
[80] H. A. Posch, H. D. Dardy, and T. A. S. Litovitz, Ber. Bunsenges. Physik. Chemie **88**, 744 (1977).
[81] R. H. Ewell, J. Appl. Phys. **9**, 252 (1938).
[82] J. B. Segur and H. E. Oberstar, Ind. Eng. Chem. **43**, 2117 (1951).
[83] R. Piccirelli and T. A. Litovic, J. Acoust. Soc. Am. **29**, 1009 (1957).
[84] L. Börjesson, M. Elmroth, and L. M. Torell, Chem. Phys. **149**, 209 (1990).
[85] W. M. Du, G. Li, H. Z. Cummins, M. Fuchs, J. Toulouse, and L. A. Knauss, Phys. Rev. E **49**, 2192 (1994).
[86] A. Bondeau and J. Huck, J. Phys. (France) **46**, 1717 (1985).
[87] Z. Chen, C. A. Angell, and R. Richert, Eur. Phys. J. E **35**, 65 (2012).

[88] J. C. Mauro, Y. Yue, A. J. Ellison, P. K. Gupta, and D. C. Allan, Proc. Natl. Acad, Sci. U.S.A. **106**, 19780 (2009).
[89] C. A. Angell and W. Sichina, Ann. N. Y. Acd. Sci. **279**, 53 (1976).
[90] L.-M. Wang, C. A. Angell, and R. Richert, J. Chem. Phys. **125**, 074505 (2006).
[91] K.L. Ngai, P. Lunkenheimer, C. León, U. Schneider, R. Brand, and A. Loidl, J. Chem. Phys. **115**, 1405 (2001).
[92] S. Hensel-Bielowka and M. Paluch, Phys. Rev. Lett. **89**, 025704 (2002).
[93] J. C. Dyre and N. B. Olsen, Phys. Rev. Lett. **91**, 155703 (2003).
[94] M. Paluch, C. M. Roland, S. Pawlus, J. Zioło, and K. L. Ngai, Phys. Rev. Lett. **91**, 115701 (2003).
[95] K. L. Ngai, K. Grzybowska, A. Grzybowski, E. Kaminska, K. Kaminski, M. Paluch, and S. Capaccioli, J. Non-Cryst. Solids **354**, 5085 (2008).
[96] R. Brand, P. Lunkenheimer, U. Schneider, and A. Loidl, Phys. Rev. B **62**, 8878 (2000).
[97] U. Bengtzelius, W. Götze, and A. Sjölander, J. Phys. C **17**, 5915 (1984).
[98] E. Leutheusser, Phys. Rev. A **29**, 2765 (1984).
[99] W. Götze and L. Sjögren, Rep. Progr. Phys. **55**, 241 (1992).
[100] W. Götze, J. Phys.: Condens. Matter **11**, A1 (1999).
[101] W. Knaak, F. Mezei, and B. Farago, Europhys. Lett. **7**, 529 (1988).
[102] N. J. Tao, G. Li and H. Z. Cummins, Phys. Rev. Lett. **66**, 1334 (1991).
[103] G. Li, W. M. Du, X. K. Chen, H. Z. Cummins, and N. J. Tao, Phys. Rev. A **45**, 3867 (1992).
[104] G. Li, W. M. Du, A. Sakai, and H. Z. Cummins, Phys. Rev. A **46**, 3343 (1992).
[105] J. Wuttke, J. Hernandez, G. Li, G. Coddens, H. Z. Cummins, F. Fujara, W. Petry, and H. Sillescu, Phys. Rev. Lett. **72**, 3052 (1993).
[106] A. P. Sokolov, W. Steffen, and E. Rössler, Phys. Rev. E **52**, 5105 (1995).
[107] P. K. Dixon, N. Menon, and S. R. Nagel, Phys. Rev. E **50**, 1717 (1994).
[108] P. Lunkenheimer, A. Pimenov, M. Dressel, Yu G. Goncharov, R. Böhmer, and A. Loidl, Phys. Rev. Lett. **77**, 318 (1996).
[109] P. Lunkenheimer, A. Pimenov, and A. Loidl, Phys. Rev. Lett. **78**, 2995 (1997).
[110] P. Lunkenheimer and A. Loidl, in *Broadband Dielectric Spectroscopy* (F. Kremer and A. Schönhals, eds.), Springer, Berlin, 2003, p. 131.
[111] P. Lunkenheimer, A. Pimenov, M. Dressel, B. Gorshunov, U. Schneider, B. Schiener, and A. Loidl, Am. Chem. Soc. Symp. Ser. **676**, 168 (1997).
[112] W. Götze, A. P. Singh, and Th. Voigtmann, Phys. Rev. E **61**, 6934 (2000).
[113] T. Franosch, M. Fuchs, W. Götze, M. R. Mayr, and A. P. Singh, Phys. Rev. E **56**, 5659 (1997).
[114] R. Schilling and T. Scheidsteger, Phys. Rev. E **56**, 2932 (1997).
[115] J. Wuttke, M. Ohl, M. Goldammer, S. Roth, U. Schneider, P. Lunkenheimer, R. Kahn, B. Rufflé, R. Lechner, and M. A. Berg, Phys. Rev. E. **61**, 2730 (2000).
[116] W. Götze and T. Voigtmann, Phys. Rev. E **61**, 4133 (2000).
[117] P. Lunkenheimer, R. Wehn, M. Köhler, and A. Loidl, preprint, arXiv:1802.06040.
[118] A. J. Martin and W. Brenig, Phys. Status Solidi B **64**, 163 (1974).
[119] V. K. Malinovsky and A. P. Sokolov, Sol. Stat. Commun. **57**, 757 (1986).
[120] V. K. Malinovsky, V. N. Novikov, P. P. Parshin, A. P. Sokolov, and M. G. Zemlyanov, Europhys. Lett. **11**, 43 (1990).
[121] U. Buchenau, N. Nücker, and A. J. Dianoux, Phys. Rev. Lett. **53**, 2316 (1984).
[122] U. Buchenau, Yu. M. Galperin, V. L. Gurevich, and H. R. Schober, Phys. Rev. B **43**, 5039 (1991).
[123] R. Orbach, Science **231**, 814 (1986).
[124] S. R. Elliott, Europhys. Lett. **19**, 201 (1992).
[125] W. Schirmacher, G. Diezemann, and C. Ganter, Phys. Rev. Lett. **81**, 136 (1998).
[126] W. Schirmacher, G. Ruocco, and Scopigno, Phys. Rev. Lett. **98**, 025501 (2007).
[127] L. H. Shintani and H. Tanaka, Nature Mater. **7**, 870 (2008).
[128] T. S. Grigera, V. Martin-Mayor, G. Parisi, and P. Verrocchio, Nature **422**, 289 (2003).
[129] P. Lunkenheimer and A. Loidl, Adv. Solid State Phys. **41**, 405 (2001).
[130] P. Lunkenheimer and A. Loidl, J. Non-Cryst. Solids **352**, 4556 (2006).
[131] R. Brand, P. Lunkenheimer, and A. Loidl, J. Chem. Phys. **116**, 10386 (2002).
[132] R. Wehn, P. Lunkenheimer, and A. Loidl, J. Non-Cryst. Solids **353**, 3862 (2007).
[133] A. Q. Tool, J. Am. Ceram. Soc. **29**, 240 (1946).
[134] O. S. Narayanaswamy, J. Am. Ceram. Soc. **54**, 240 (1971).
[135] G. W. Scherer, Relaxation in Glass and Composites, Wiley, New York, 1986.
[136] I. M. Hodge, J. Non-Cryst. Solids **169**, 211 (1994).
[137] R. L. Leheny and S. R. Nagel, Phys. Rev. B **57**, 5154 (1998).
[138] Y. Z. Yue, S. L. Jensen, and J. C. Christiansen, Appl. Phys. Lett. **81**, 2983 (2002).
[139] H. Yardimci and R. L. Leheny, J. Chem. Phys. **124**, 214503 (2006).

[140] C. T. Moynihan, P. B. Macedo, C. J. Montrose, P. K. Gupta, M. A. DeBolt, J. F. Dill, B. E. Dom, P. W. Drake, A. J. Easteal, P. B. Elterman, R. P. Moeller, H. Sasabe, and J. A. Wilder, Ann. N. Y. Acd. Sci. **279**, 15 (1976).
[141] P. Lunkenheimer, R. Wehn, and A. Loidl, J. Non-Cryst. Solids **352**, 4941 (2006).
[142] R. Richert, P. Lunkenheimer, S. Kastner, and A. Loidl, J. Phys. Chem. B **117**, 12689 (2013).
[143] E. Gardner, Nucl. Phys. B **257**, 747 (1985).
[144] D. J. Gross, I. Kanter, and H. Sompolinsky, Phys. Rev. Lett. **55**, 304 (1985).
[145] P. Charbonneau, J. Kurchan, G. Parisi, P. Urbani, and F. Zamponi, Nat. Commun. **5**, 3725 (2014).
[146] G. Biroli and P. Urbani., Nat. Phys. **12**, 1130 (2016).
[147] J. Kurchan, G. Parisi, P. Urbani, and F. Zamponi, J. Phys. Chem. B **117**, 12979 (2013).
[148] L. Berthier, P. Charbonneau, Y. Jin, G. Parisi, B. Seoane, and F. Zamponi, Proc. Natl. Acad. Sci. U.S.A. **113**, 8397 (2016).
[149] Y. Jin and H. Yoshino, Nat. Commun. **8**, 14935 (2017).
[150] P. Charbonneau, Y. Jin, G. Parisi, C. Rainone, B. Seoane, and F. Zamponi, Phys. Rev. E **92**, 012316 (2015).
[151] C. Scalliet, L. Berthier, and F. Zamponi, Phys. Rev. Lett. **119**, 205501 (2017).
[152] C. L. Hicks, M. J. Wheatley, M. J. Godfrey, and M. A. Moore, unpublished, arXiv: 1708.05644.
[153] T. R. Kirkpatrick and P. G. Wolynes, Phys. Rev. B **36**, 8552 (1987).
[154] M. Sperl, Phys. Rev. E **74**, 011503 (2006).